A REMARKABLE ADAPTIVE PARADIGM OF HEART PERFORMANCE AND PROTECTION EMERGES IN RESPONSE TO THE CONSTITUTIVE CHALLENGE of MARKED CARDIAC-SPECIFIC OVEREXPRESSION OF ADENYLYL CYCLASE TYPE 8

Kirill V. Tarasov[1], Khalid Chakir[1], Daniel R. Riordon[1], Alexey E. Lyashkov[2], Ismayil Ahmet[1], Maria Grazia Perino[1], Allwin Jennifa Silvester[1], Jing Zhang[1], Mingyi Wang[1], Yevgeniya O. Lukyanenko[2], Jia-Hua Qu[1], Miguel Calvo-Rubio Barrera[2], Magdalena Juhaszova [1], Yelena S Tarasova[1], Bruce Ziman[1], Richard Telljohann[1], Vikas Kumar[1], Mark Ranek[3], John Lammons[1], Rostislav Beshkov[1], Rafael deCabo[2], Seungho Jun[3], Gizem Keceli[3], Ashish Gupta[3], Dongmei Yang[1], Miguel A. Aon[1], Luigi Adamo[3], Christopher H. Morrell[1], Walter Otu[1], Cameron Carroll[1], Shane Chambers[1], Nazareno Paolocci[3], Thanh Huynh[5], Karel Pacak[5], Robert G Weiss[3], Loren Field[4], Steven J. Sollott[1] and Edward G Lakatta[1]*.

[1] LABORATORY of CARDIOVASCULAR SCIENCE, [2]TRANSLATIONAL GERONTOLOGY BRANCH, INTRAMURAL RESEARCH PROGRAM, NATIONAL INSTITUTE ON AGING, NATIONAL INSTITUTES OF HEALTH, BALTIMORE, MARYLAND,
[3] DIVISION OF CARDIOLOGY, DEPARTMENT OF MEDICINE, JOHNS HOPKINS UNIVERSITY SCHOOL OF MEDICINE, BALTIMORE, MD 21205, USA

[4] KRAENNERT INSTITUTE OF CARDIOLOGY, INDIANNA UNIVERSITY SCHOOL OF MEDICINE, INDIANAPOLIS, INDIANA

[5] SECTION ON MEDICAL NEUROENDOCRINOLOGY, EUNICE KENNEDY SHRIVER NATIONAL INSTITUTE OF CHILD HEALTH AND HUMAN DEVELOPMENT, NIH, BETHESDA, MARYLAND, USA

* Corresponding author

Abstract

Adult mice with a marked increase in Adenylyl cyclase (AC) activity due to cardio-specific over expression of adenylyl cyclase (AC) type VIII (TG^{AC8}) have an incessantly cardiac work load adapt to this chronic, severe cAMP stress for up to a year without signs of heart failure and without excessive mortality compared to wild-type littermates (WT). Here we focused on mechanisms that underly the TG^{AC8} adaptive paradigm.

Although TG^{AC8} mice had a 30% increase in both HR and cardiac output, a 23% increase in EF (echocardiography), neither total LV mass nor pathologic hypertrophy biomarkers differed by genotype. Compared to WT the LV cavity volume was reduced in TG^{AC8}, but was encased by thicker LV walls, harboring populations of both smaller cardiac myocytes, and small non-cardiac interstitial cells having increased nuclear EdU labeling. Protein synthesis, proteosome activity, autophagy, Nrf-2 and Hsp90α proteins were also increased in TG^{AC8} vs WT, but super-oxide radicals did not differ. Despite an apparently marked increased energy demand due to a chronically increased cardiac workload in the context of a chronically increased HR and EF, steady-state LV ATP and phosphocreatine in vivo did not differ in TG^{AC8} vs WT. Further Acc2, known to suppress fatty acid oxidation and to increase aerobic glycolysis in the context of enhanced utilization of the pentose phosphate shunt, and NADH/NADPH cycling were both elevated in TG^{AC8} vs WT mice.

Unbiased omics unveiled additional genotypic differences in the potential mechanisms involved in the chronically increased TG^{AC8} heart performance and the adaptive paradigm in response to this chronic stress. 2,323 transcripts and 2,184 proteins, spanning a wide array of biological processes and molecular functions in numerous cellular compartments, including over 250 canonical signaling pathways, that integrate stress responses, cytokine and T cell receptor

signaling, immune responses, ROS scavenging, protection from apoptosis, and nutrient sensing, were activated in TG^{AC8} vs WT. Several adaptive mechanisms that limit cAMP/PKA signaling were also activated in TG^{AC8}.

Thus, in addition to markedly increased cardiac work, the chronic, intense AC-PKA-Ca^{2+} signaling within the adult TG^{AC8} heart concurrently activates a consilience of adaptive mechanisms within the TG^{AC8} LV that resemble survival mechanisms within cancer cells.

Introduction

Adaptations have evolved in all organisms to cope with both acute and chronic internal and environmental stress. For example, even during acute exercise increased autonomic sympathetic-mediated AC/cAMP/PKA/Ca^{2+} signaling, the quintessential mediator of both acute and chronic stress, also activates acute physiologic adaptations to moderate the exercise-induced increase in sympathetic signaling. In response to repeated bouts of acute exercise induced AC/cAMP/PKA/Ca^{2+} stress chronic adaptations emerge (endurance exercise conditioning).[1,2,3]

Prolonged and intense chronic cAMP-mediated stress in experimental animal models results in cardiomyopathy and death.[4,5] During chronic pathophysiologic states e.g. chronic heart failure (CHF) in humans, AC/cAMP/PKA/Ca^{2+} signaling progressively increases as the degree of heart failure progresses, leading to cardiac inflammation, mediated in part, by cyclic-AMP-induced up- regulation of renin-angiotensin system (RAS) signaling. Standard therapies for CHF include β-adrenoreceptor blockers and RAS inhibitors,[6,7] which although effective, are suboptimal in amelioration of heart failure progression.

One strategy to devise novel and better therapies for heart failure, would be to uncover the full spectrum of consilient cardio- protective adaptations that can emerge in response to severe, chronic AC/cAMP/PKA/Ca^{2+} -induced cardiac stress. The young adult TG^{AC8} heart in which cardiac-specific over expression in mice of Adenylyl Cyclase (AC) Type 8, driven by the α myosin heavy chain promoter, markedly enhances AC activity and cAMP signaling, may be an ideal model in which to elucidate the features of a wide-spread an adaptive paradigm that must become engaged in response to incessant chronic activation of cardiac AC/cAMP/PKA/Ca^{2+} signaling. Specifically, concurrent with chronically increased AC activity within the young adult TG^{AC8} sinoatrial node

(SAN) and LV,[8,9] increased heart rate (HR), measured via telemetry in the awake, unrestrained state, increased by approximately 30%, persisting in the presence of dual autonomic blockade;[8] and LV EF is also markedly increased in TG^{AC8}.[10] Thus, the cardiac phenotype of the adult TG^{AC8} mimics cardiac responses to AC/cAMP/PKA/Ca^{2+} sympathetic autonomic input during strenuous, acute exercise, but this stressful state persists incessantly. [8] Although this incessant high cardiac load imposes a severe chronic stress on the heart that might be expected to lead to the near term heart failure and demise,[11, 12] adult TG^{AC8} mice maintain this remarkable, hyperdynamic cardiac phenotype up to about a one year of age,[9,13,14,10] when signs of CHF begin to develop and cardiomyopathy ensues.[10]

We hypothesized, (1) that a panoply of intrinsic adaptive mechanisms become *concurrently* engaged in order to protect the TG^{AC8} heart during the incessant, high level of cardiac work in several months, and (2) that, some of these mechanisms are those that become activated in the endurance, trained heart, including shifts in mechanisms of energy generation, enhanced protein synthesis and quality control, and increased defenses against reactive O_2 species (ROS) and cell death.[15,16] We reasoned that a discovery bioinformatics approach in conjunction with a deeper phenotypic characterization of TG^{AC8} LV, would generate a number of testable hypotheses about the characteristics of some of these mechanisms utilized to sustain this adaptive paradigm of heart performance and protection in response to severe, chronic adenylyl cyclase-induced cardiac stress. To this end, we performed unbiased, RNASEQ and proteomic analyses of adult TG^{AC8} and WT LVs, and selectively validated genotypic differences in numerous transcripts and proteins. Our results delineate an emergent consilient pattern of adaptations within the TG^{AC8} heart in response to chronically increased AC/cAMP/PKA/Ca^{2+}-signaling and offer numerous testable hypotheses

to further define the details of mechanisms that underlie what we will show here to be a remarkable adaptive heart paradigm.

Materials and Methods

Mice

All studies were performed in accordance with the Guide for the Care and Use of Laboratory Animals published by the National Institutes of Health (NIH Publication no. 85-23, revised 1996). The experimental protocols were approved by the Animal Care and Use Committee of the National Institutes of Health (protocol #441-LCS-2019). A breeder pair of TG^{AC8} over expression mice, generated by ligating the murine α-myosin heavy chain promoter to a cDNA coding for human TG^{AC8}, were a gift from Nicole Defer/Jacques Hanoune, Unite de Recherches, INSERM U- 99, Hôpital Henri Mondor, F-94010 Créteil, France.[9] Mice were bred adult (3 mo) and housed in a climate-controlled room with 12-hour light cycle and free access to food and water, as previously described.[8]

Detailed methodology for RNASEQ and LV Proteome analyses, WB and RT-qPCR analyses, echocardiography, heart and cardiac tissue isolation, isolated perfused working heart experiments, nuclear EdU and BrdU uptake in cells within LV tissue, adenyl cyclase activity, immunohistochemistry, protein synthesis, misfolding and degradation, autophagy, NMR spectroscopy, transmission electron microscopy, mitochondrial permeability transition threshold, are provided in the online supplement.

Results

Cardiac Structure and Performance.

We performed echocardiography and cardiac histology for in-depth characterization of the TG^{AC8} heart structure and function. Representative echocardiograms of TG^{AC8} and WT are illustrated in **Fig.S1**, selected Echo parameters are shown in **Fig 1**, (and a complete listing of parameters is provided in **Table S.1)**. Both EF and HR were higher in TG^{AC8} than in WT (**Fig 1 A, B**), confirming prior reports.[8,10] Because stroke volume did not differ by genotype (**Fig 1C**), cardiac output was elevated by 30% in TG^{AC8} (**Fig 1D**) on the basis of its 30% increase in HR. Arterial blood pressure was only mildly increased in TG^{AC8} averaging 3.5 mmHg higher than in WT (**Fig 1E**).

A sustained high cardiac workload is usually expected to result in an increase of a total LV mass,[1,17,18] i.e., cardiac hypertrophy. Although both the LV posterior wall and inter-ventricular septum were thicker in TG^{AC8} vs WT (indicative of an increased LV wall biomass), (**Fig 1 F, G**) the LV cavity volume was markedly reduced (**Fig 1 H, I**), and the echo derived **total** LV mass did not differ by genotype (**Fig 1 J**). Postmortem measurements indicated that although the body weight did not differ between TG^{AC8} and WT (**Fig 1 K**), the heart weight/body weight (HW/BW) was even actually, modestly reduced in TG^{AC8} vs WT (**Fig 1 L**).

Pathological hypertrophy markers e.g., β-myosin heavy chain (MYH7), ANP (NPPA) or BNP (NPPB) were not increased in TG^{AC8} vs WT by Western Blot (WB) (**Fig 2A**); curiously, α skeletal actin, commonly considered to be a pathologic hypertrophy marker, was increased in TG^{AC8} vs WT (**Fig 2A**). Calcineurin (PP2B), which activates the hypertrophic response by

dephosphorylating nuclear factor of activated T cells (NFAT),[19] did not differ in WB of TG^{AC8} vs WT (**Fig 2A)**.

LV Histologic Analysis

The average LV cardiac myocyte size was smaller in TG^{AC8} compared to WT (**Fig 2 B, C**), and LV myocyte size distribution was different by genotype (**Fig 2 D**). LV collagen content in TG^{AC8} was not increased vs WT (**Fig S. 2).**

To address the issue of DNA synthesis within LV cardiac myocyte we loaded EdU for 28-days. EdU labeled nuclei, detected in both TG^{AC8} and WT whole mount ventricular preparations were randomly scattered throughout the LV from the mitral annulus to the apex. LV myocyte nuclei, however, were rarely EdU labeled. Rather nearly all EdU labelling was detected in small interstitial cells that expressed vimentin or in cells that enclosed the capillary lumina (**Fig 3 A-G)**, suggesting that EdU was also incorporated within the DNA of endothelial cells in both WT and TG^{AC8}. However, total nuclear EdU labeling was 3-fold higher in TG^{AC8} than in WT **Fig 3 H**.

To monitor cardiomyocyte S-phase activity, TG^{AC8} mice were crossed with MHC-nLAC mice (which express a nuclear-localized β-galactosidase reporter under the transcriptional regulation of the mouse α-cardiac MHC promoter; these mice are useful to identify cardiomyocyte nuclei in histologic sections).[20] The resulting TG^{AC8}, MHC-nLAC double-transgenic mice and MHC-nLAC single-transgenic mice were identified and sequestered. At 28-to-30 days of age, the mice were administered BrdU via drinking water (0.5 mg/ml, changed every 2nd day) for a total of 12 days. There was no difference in the level of ventricular cardiomyocyte S-phase activity in the TG^{AC8}, MHC-nLAC double-transgenic vs. the MHC-nLAC single transgenic animals (**Fig 3 H-K**).

Thus, the adult TG^{AC8} heart has a hyper-dynamic LV with thicker walls, harboring not only an increased number of small **cardiac** myocytes, but also an increased number of small interstitial cells and endothelial cells with increased EdU labeling vs WT. The LV cavity volumes at both end-diastole and end-systole were markedly reduced, and LV EF was markedly increased in TG^{AC8} vs WT. But, neither **total** LV mass, nor collagen content were increased in TG^{AC8} vs WT and the profile of pathologic cardiac hypertrophy markers in TG^{AC8} was absent.

AC/cAMP/PKA/Ca^{2+} signaling

Given that the transgene in our study was an AC, we next focused on expected differences in AC/cAMP/PKA/Ca^{2+} signaling in TG^{AC8} vs WT. Immunolabeling of single LV myocytes showed that AC8 expression was markedly increased (by 8-9-fold in TG^{AC8} vs WT), and AC activity (measured in membranes isolated from LV tissue) in TG^{AC8} was 50% higher than that in WT (**Fig 4 A-C**). Expression of the PKA catalytic subunit was increased by 65.6%, and expression of the regulatory subunit was decreased by 26.7% in TG^{AC8} by WB (**Fig 4 D, E**). PKA activity was increased by 57.8 % in TG^{AC8} vs WT (**Fig 4 F**).

To search for mechanisms that increase contractility within cardiac myocytes we examined the expression of selected proteins downstream of PKA signaling that are involved in excitation/Ca^{2+} release/contraction/relaxation. Western Blot analysis revealed that a number of proteins that determine increase cardiac myocyte performance were upregulated in TG^{AC8} vs WT, including αMHC (MYH6 by 18.7%), SERCA2 (ATP2A2 by 62.0%), L-type Ca Channel (Cav1.2, by 61.8%), and NCX1 (AKA SLC8A1) by 117.6%, and CaMKII by 35.0% (**Fig 4 G-K**). Immunolabeling of total RyR2 was increased by 66% in TG^{AC8} vs WT (**Fig 4 L**). This pattern of increased protein expression consistent with increased Ca^{2+} flux into and out of cardiac myocytes,

an increased Ca^{2+} cycling between SR and cytosol, and increased myosin cross-bridge kinetics during heart contraction in TG^{AC8} vs WT.

Thus, as would be expected in the context of markedly increased transcription of AC type VIII, AC and PKA protein levels and activities, and levels of proteins downstream of PKA signaling were markedly increased and associated with a chronic, marked increase in LV performance.

Myocardial and plasma catecholamines.

It is well known, that PKA signaling activates a cascade of enzymes beginning with tyrosine hydroxylase (TH), that results in a production of catecholamines (**Fig S.3 A**). Among these enzymes, dopamine decarboxylase, which converts DOPA to dopamine, was increased in TG^{AC8} vs WT (**Fig S.3 B**), dopamine b-hydroxylase, which converts dopamine to norepinephrine did not differe by genotype, and phenylethanolamine N-methyltransferase (PNMT), which converts norepinephrine to epinephrine was reduced in TGAC8 vs WT. In the context of these genotypic differences in enzyme levels LV tissue dopamine was increased and DHPG was reduced and NE was borderline reduced (p=0.08) **Fig S.3 B**.

Interestingly, as noted previosly [8], plasma levels of dopa and dopamine were also incresed in TG^{AC8} vs WT, whereas norepinephrine, epinephrine, DOPAC and DHPG were reduced (**Fig S.3 C**).

Protein Synthesis, Degradation and Quality Control

Because PKA signaling-driven increased cardiac work is known to be associated with increased protein synthesis,[21, 22] we next compared the rate of protein synthesis in TG^{AC8} and WT LV lysates. Despite the absence of increase of total LV mass, the rate of protein synthesis was

40% higher in TG^{AC8} than in WT (**Fig 5 A**). WB analysis indicated that expression or activation of p21Ras, p-c-Raf, MEK1/2, molecules downstream of PKA signaling that are implicated in protein synthesis, were increased in TG^{AC8} vs WT (**Fig 5 B-C**). The transcription factor CREB1, involved in PKA signaling directed protein synthesis was increased by 58.1% in TG^{AC8} vs WT in WB analysis (**Fig 5 D).** Expression of CITED4 (family of transcriptional coactivators that bind to several proteins, including CREB-binding protein (CBP)) was increased by 51 % in TG^{AC8} vs WT in WB analysis (**Fig 5 E).** Expression of protein kinases, that are required for stress-induced activation of CREB1, MSK1 and MNK1, direct substrates of MAPK, were increased by 40% and 48% respectively in TG^{AC8} vs WT (**Fig 5 F** and **G**).

Autophagy

Proteasome activity within LV lysates was increased in TG^{AC8} vs WT **(Fig 6 A)**. However, although there was a significant increase in the amount of soluble misfolded proteins in TG^{AC8} vs WT **(Fig 6 B)**, insoluble protein aggregates did not accumulate within the TG^{AC8} LV (**Fig 6 C**). This suggest that an increase in micro-autophagy of the TG^{AC8} LV circumvents the potential proteotoxic stress of aggregated protein accumulation, which can negatively impact cardiac cell health and function. A 24% increase in the expression of HSP90α (**Fig 6 D**) in TG^{AC8} also suggested that chaperone-mediated autophagy was involved in preventing an accumulation of insoluble protein aggregates.

We reasoned that another type of protein quality control, macro-autophagy, might also be activated in TG^{AC8} vs WT. Indeed, protein levels of several members of the autophagy machinery were increased in TG^{AC8} vs WT: both ATG13, a factor required for autophagosome formation and mitophagy, and the ubiquitin-protein ligase PARKIN, which protects against mitochondrial dysfunction during cellular stress, by coordinating mitochondrial quality control mechanisms in

order to remove/replace dysfunctional mitochondrial components, were significantly increased in TG^{AC8} vs WT (**Figure 6 E, F)**. Furthermore, protein levels of the cysteine protease ATG4B, involved in processing, and the lipidation/delipidation steps (conjugation/removal of phosphatidylethanolamine) and insertion of MAP1LC3, GABARAPL1, GABARAPL2 and GABARAP into membranes, during autophagy and endocytosis, were also increased (**Fig 6 G)**. In addition, the catalytic subunit of the PI3Kc3, involved in initiation and maturation of autophagosomes and in endocytosis, was also significantly higher in the TG^{AC8} vs WT (**Fig 6 H)**. Finally, direct measurements in single LV myocytes showed that autophagolysosomes were appreciably increased in TG^{AC8} vs WT, indicating that autophagy (mitophagy) was activated to the greater extent in the TG^{AC8} vs WT. (**Fig 6 I, J)**.

Mitochondrial Structure

We employed transmission electron microscopy (TEM) to directly visualize ultrastructural details of the mitochondria and cardiac myofibers in the LVs of TG^{AC8} and WT. Representative panoramic electron micrographs of LV cardiac muscle fibers and mitochondria in TG^{AC8} and WT are illustrated in **Fig 7 A and B**. Cardiac myocytes presented a very distinctive morphology with high content of myofibrils and a large number of high-electron dense mitochondria and several capillaries surrounding cardiac myocytes are depicted (see white arrows). Cardiac myocyte ultrastructure is depicted in **Fig 7** panels **C** and **E**, for WT mice, and in panels **D** and **F**, for TG^{AC8}. Asterisks show swollen, disrupted mitochondria with lighter cristae compared to the surrounding healthy mitochondria. **Fig 7** Panels **G-J** present quantitative stereological analyses of normal and damaged mitochondria. Although there was a mild increase in the number of damaged mitochondria (0.3 %), and in the percent of cell volume occupied by damaged mitochondria (0.4%) in TG^{AC8}, the numbers of healthy mitochondria and the percent of cell volume occupied by healthy

mitochondria did not differ between TG^{AC8} and WT. Nevertheless, the presence of mitochondrial deterioration at a young age is uncommon and may be further evidence for enhanced cleaning and recycling mechanisms such as autophagic signaling, (**Figs 6, 7**).

Mitochondrial Fitness

The healthy functioning and survival of cardiac myocytes during severe, chronic myocardial stress requires close coordination of survival mechanisms and numerous mitochondrial functions that require a high level of mitochondrial fitness.[23,24,25,26] The mitochondrial permeability transition pore (mPTP) is a key regulator of mitochondrial functions, including energy metabolism (e.g., with the pore performing as a "safety valve", opening transiently and reversibly, to prevent: 1) the excessive accumulation of certain regulatory species, such as Ca^{2+}; and 2) bioenergetic byproducts/damaging reactive species, such as free radicals, from achieving toxic levels. The mPTP also regulates cell fate: enduring and irreversible pore opening, plays decisive mechanistic roles in mitochondrial and cell life vs death decisions during normal development or pathological stress (e.g., involving excess and damaging free radical exposure). Measurement of the pore susceptibility or resistance to being induced/opened can serve as a biomarker of mitochondrial fitness. **Fig 7** panels **M** and **N** shows that the mPTP ROS threshold did not differ in TG^{AC8} vs WT, suggesting a comparable degree of mitochondrial fitness in both genotypes.

ROS levels and NRF Signaling.

Given the incessantly elevated myocardial contractility and heart rate, and increased protein synthesis and quality control mechanisms in TG^{AC8} vs WT, it might be expected that ROS levels are increased in TG^{AC8}. To this end we measured of superoxide radical accumulation in isolated, perfused, isometrically contracting TG^{AC8} hearts that maintained markedly enhanced cardiac workload observed *in vivo* (**Fig 8 A-B)**. Superoxide radical accumulation did not differ by

genotype**,** suggesting that mechanisms to scavenge ROS are increased in TG^{AC8}. Indeed, the level of NRF2 protein, a key regulator of ROS defense signaling was increased by 24% in TG^{AC8} vs WT, suggesting that increased NRF signaling in the TG^{AC8} LV may be a factor that prevents the accumulation of superoxide ROS.

High Energy Phosphates.

Given the fact, that increased protein synthesis and quality control mechanisms **(Fig 6**), maintenance of normal ROS levels (**Fig 8**) and the incessant high cardiac performance of the TG^{AC8} (**Fig 1)** require increased energy production**,** it is reasonable to assume that the total energy requirements of the TG^{AC8} LV are probably considerably higher than those in WT. It was important, therefore, to assess high energy phosphate levels in TG^{AC8} and WT. A schematic of ATP-creatine energy system is depicted in **Fig 9A**. Steady state levels of ATP, phosphocreatine and the ATP: phosphocreatine assessed in *vivo,* were maintained at the same level in TG^{AC8} as in WT (**Fig 9 B-E**), suggesting that the rate of ATP production in the TG^{AC8} LV is adequate to meet its increased energy demands at least when animals rest.

Unbiased RNASEQ and Proteome Analyses

We performed unbiased, RNASEQ and proteome analyses of adult TG^{AC8} and WT left ventricles (LV) in order to realize facets of the consilience of adaptive mechanisms beyond those, identified in our experiments illustrated in **Figs 1-9**. We reasoned that taking advantage of the knowledge base within bioinformatic tools would also generate a number of testable hypotheses regarding the components of adaptive paradigm of heart performance and protection in response to the constitutive challenge of marked cardiac-specific overexpression adenylyl cyclase type 8.

LV Transcriptome (RNASEQ)

RNA sequencing identified 11,810 transcripts in LV lysates (**Fig 10 A**, **Table S.2**); of these, 2,323 were differentially expressed in TG^{AC8} vs WT (**Fig 10 A** and T**able S.3**): 1,201 were significantly upregulated in TG^{AC8} vs WT, and 1,117 were significantly downregulated. A volcano plot and heatmap of these transcripts are shown in **Fig S.4 panels A and C**. The transcript abundance of human *ADCY8* in TG^{AC8} (LV) myocardium was more than 100-fold higher than the endogenous mouse isoform (**Figure S.4 E**).

The LV Proteome

6,834 proteins were identified in the LV proteome (**Fig 10 A**, **Table S.4**); of these, 2,184 were differentially expressed (**Table S.5**) in TG^{AC8} vs WT: 2,026 were upregulated and 158 were downregulated in TG^{AC8}. A Volcano plot and heatmap of the proteome are shown in the **Fig S.4** panels **B and D**.

Bioinformatic Analyses of the *Total* Transcriptome and Proteome Datasets

We employed WEB-based GEne SeT AnaLysis Toolkit (WebGestalt) and Ingenuity Pathway Analysis (IPA), online platforms for in depth analyses of the total 2,323 expressed transcripts (**Fig 10 A-a**) and the total 2,184 **(Fig 10 A-b)** proteins that differed by genotype.

In Gene Ontology (GO) analysis WebGestalt classifies submitted molecules into three main categories, i.e., Biological Process (BP), Cellular Component (CC), Molecular Function (MF), (**Figure 10 B)**. Remarkably, transcriptome and proteome gene ontology (GO) terms that differed by genotype in response to overexpression of a single gene, AC Type 8, covered nearly all the biological processes and molecular functions within nearly all compartments of the TG^{AC8} LV myocardium.

In order to discover genotypic differences in canonical signaling pathway enrichment, we performed QIAGEN Ingenuity Pathway Analysis (IPA) of the total number of transcripts (2,323) that were differentially expressed by genotype **(Fig 10 A-c)** and the total number of proteins (2,184 **Fig 10 A-d**). In IPA analyses 248 canonical pathways in the transcriptome analyses and 308 canonical pathways in the proteome differed by genotype $p<0.05$ in *enrichment* (listed in **Tables S. 6A, B**). 154 pathways in transcriptome or proteome were *activated* by genotype (Z-score calculated) and Spearman's correlation coefficient r_s was 0.57, $p < 0.0001$ **Fig S.5**, and showed moderate correlation between enriched and activated pathways in transcriptome and proteome

Although 60 molecules were represented in only a single enriched pathway, 22 molecules were represented in 10 or more pathways, the highest among these being: MAP3K – (68 pathways); MAP2K2 – (51 pathways); and PLCG2 – (33 pathways) (**Table S.6C**). Representation of several differentially expressed molecules in multiple canonical signaling pathways that differed by genotype is a plausible explanation accounting for the consilient pattern of pathway enrichment and activation in the TG^{AC8} heart identified in IPA analyses.

The top enriched and activated or inactivated pathways are illustrated in **Fig 10 C**. Of note, several pathways, e.g., Nrf2 signaling, Integrin Signaling, and Cardiac Hypertrophy Signaling were among the top activated pathways that were highly enriched in TG^{AC8} vs WT, whereas fatty acid β-oxidation, tryptophan degradation III, isoleucine degradation and glutaryl Co-A degradation were markedly suppressed in TG^{AC8} vs WT (**Fig 10 C**). Surprisingly, the top differentially regulated pathways between TG^{AC8} and WT was "leukocyte extravasation signaling" (**Fig 10 C**).

Bioinformatic Analyses of Transcripts and Proteins that *Both* Significantly Differed by Genotype

544 transcripts and proteins **both** differed by genotype **(Fig 9A-e, Table S.7A)**. Of these 544, 339 (62.32%) were significantly **upregulated** in TG^{AC8}; and 99 (18.2%) were significantly downregulated in TG^{AC8}. Thus, of the 544 transcripts and proteins that **both** significantly differed by genotype, 80.5% differed **concordantly** (in the same direction, **Fig S.6**).

We next subjected these 544 molecules to IPA analysis. 170 of the **same** canonical pathways in the transcriptome and proteome differed by genotype in enrichment. Of these, 118 pathways also differed by genotype and activation status (**Table S.7B**).

In addition to IPA analyses we also used PROTEOMAP platform[27] to visualize functional categories of the 544 proteins that differed by genotype in **Fig 10 A-e, Fig S.6**. PROTEOMAP displays a protein data set as functional trees (**Fig S.7**), each consisting of a number of polygons, the areas of which reflect genotypic differences in protein abundances. Genotypic differences were most marked by increases in TG^{AC8} of: ENVIRONMENTAL INFORMATION PROCESSING (informing on marked differences by **Rap1** and **PI3K-AKT** signaling pathways, harboring the marked increases in expression of ADCY8 and TNC (tenascin) proteins); GENETIC INFORMATION PROCESSING (informing on PROTEIN **translation, folding, sorting and degradation** signaling pathways, harboring marked increases in RNF128, MMP2 and WFS1); and CELLULAR PROCESSES (informing on **vesicular transport** and **exosome**, harboring increased NCF1, LCP1 and CTSZ proteins).

PROTEOMAP also identified major genotypic changes in BIOSYNTHESIS AND CENTRAL CARBON METABOLISM (**Fig S.7**), informing on genotypic differences in:

membrane transport, harboring increased SLC4A2 (regulates intracellular pH, biliary bicarbonate secretion, and chloride uptake); **other metabolic enzyme proteins** (PDK3, SULF2 and ALPK2), and carbohydrate metabolism; and **glycolysis**, harboring reduced ALDH1B1.

Regulatory Networks Centered on cAMP and Protein Kinase A Signaling

Having confirmed that both AC8 protein and AC activity were markedly increased in TG^{AC8} vs WT (**Fig 4 B, C**) it was reasonable to infer that the multitude of genotypic differences that were identified in WebGestalt, IPA and PROTEOMAP (**Figs 10 B, S6; Table S.6**) might be ultimately (directly or indirectly) linked to increased signaling driven by the high levels of AC activity. Three main downstream targets of cAMP generated by AC activity are: protein kinase A (**PKA**), guanidine-nucleotide exchange proteins activated by cAMP (**EPACs**), and cyclic nucleotide-gated ion channels (**CNGCs**). We found no evidence of activation for 2 of these 3 targets. In fact: 1) Neither CNGC subunits α 1-4, nor β 1-2 transcripts or proteins were identified in our omics analysis; 2) omics analysis (**Table S.2, S4**) provided no evidence to suggest that cAMP directed **Epac** signaling was upregulated in the TG^{AC8} LV. More specifically, transcripts of *Rapgef* 1 thru 6 were significantly **downregulated** in TG^{AC8} vs WT (**Table S.3**) and RAPGEF 2, 3 and 5 proteins identified in proteomic analyses did not differ by genotype (**Table S.4**). On the contrary, we found clear evidence of activation of PKA. In fact, we had shown that PKA catalytic subunit and PKA activity are substantially higher in TG^{AC8} vs WT (**Fig 4 D, F**), and PKA signaling was among the top pathways increased and activated in IPA analysis We therefore next focused the IPA knowledge base on the PKA complex as the center of a number of **interacting** pathways. We noticed that in addition to cAMP, another upstream regulator of PKA signaling, ITGA5, was increased in TG^{AC8} vs WT in both the transcriptome and proteome (**Fig 11**), suggesting increased crosstalk between intra and extra cellular signaling.

To further investigate the role of PKA-signaling in the extreme TG^{AC8} phenotype, we next established the protein interaction network centered on PKA (**Fig 11**). Gene families of these proteins ranged from transcription regulators, kinases, peptidases and other enzymes to transmembrane receptors, ion channels and other protein families (CFH, CD44, HOMER1, and SERPINF1). Although CREB1 protein was not identified in proteome analyses, as noted this canonical transcription factor, and its phosphorylated form activated by PKA were markedly increased in WB analyses (**Figs 5 D**, **S.11 B**). Canonical signaling pathways in which these proteins operate and downstream biological and molecular processes of proteins in these pathways are listed in **Fig. 11** (lower part). See **Table S.8** for the full list of these downstream effects.

Shifts in Metabolism

The enrichment or activation of the large number of signaling pathways in TG^{AC8} vs WT (**Fig 10 C, S.6; Table S.6 A, B**) suggested that some aspects of metabolism differed by genotype. A detailed schematic of the genotypic differences in transcripts and proteins that related to metabolism circuits is illustrated in **Fig 12,** and WB validations of selected proteins are presented in **Fig S.8.** Bioinformatic analyses suggested that nutrient sensing pathways, including AMPK, insulin and IGF signaling, that induce shifts in aerobic energy metabolism were activated in TG^{AC8} vs WT LV. A close inspection of the bioinformatic analyses of central carbon metabolic processes (**Fig 12**) suggested that catabolism of glucose is markedly increased in TG^{AC8} vs WT, while the fatty acid β oxidation pathway is concurrently reduced.

An increase in myocardial glucose metabolism in TG^{AC8} vs WT was suggested by increases in GLUT1, HK1, GSK3B, GYS1 and PFK, PGK1, PGA and PKM. Interestingly, bioinformatic analyses suggested that, both transcript (down by 86%) and protein (down by 38%) expression of ALDOB were reduced in TG^{AC8} vs WT. Signals related to reduced fatty acid oxidation (FAO)

likely stem from reductions in CPT1, CPT2, ACAT1, HADH, HADHA, and HADHB (**Fig 12**). Further, signals from bioinformatic analyses pointed to reduced utilization of the TCA cycle and mitochondrial respiration within the TG^{AC8} LV vs WT **(Fig 12)**. Interestingly omics signals suggested that the malate-aspartate shuttle (MAS), which results in the net transport H+ from cytosol back to the mitochondria, may be suppressed in TG^{AC8} vs WT, because transcripts of *Ldhb*, *Mpc1, Mpc2, Mdh1, Got1, Slc25a11 Slc25a13*, and SLC25A13 protein was also downregulated (**Figs 12, S.9**)

The results of bioinformatic analyses also pointed to increased expression, in TG^{AC8} vs WT, of the glucose transporter, lactic acid dehydrogenase type A and the glutamine transporter, that are required for enhanced aerobic glycolysis[28] (**Fig 12**). **Enhanced growth factor** and other PI3K/AKT driven signaling processes in TG^{AC8} suggested by omics analyses (**Fig 12)** and validated by WB (**Fig S.8)** are tightly linked to aerobic glycolysis and utilization of pentose phosphate shunt (PPS).[28] Increased utilization of the PPS in TG^{AC8} vs WT is suggested by increases in both the expression of transcripts and proteins of G6PDH, PGD and PRPS2 (**Fig 12**).

Because Acetyl-CoA carboxylase (ACC), a complex multifunctional enzyme system that catalyzes the carboxylation of acetyl-CoA to malonyl-CoA, which limits CPT1 transport of FA into the mitochondria, we inquired whether, in addition to reduction in CPT1 transcripts and reductions in CPT1 and CPT2 proteins in TG^{AC8} vs WT, ACC2 might also be increased in TG^{AC8} LV myocytes. Indeed, immunolabeling of isolated LV cardiomyocytes indicated a clear increased in ACC2 (AKA ACACB) protein expression (**Fig S.10 A**); and in increase *Acc1* (AKA *Acaca*) mRNA was documented in LV tissue by RT-qPCR (**Fig S.10 B**). Such an increase of ACC2 expression in TG^{AC8} may not only explain a shift from FAO to glucose utilization within the TG^{AC8} LV but may also explain increased utilization of Aerobic glycolysis in TG^{AC8} vs WT, which is

linked enhanced utilization of PPS to increase anabolic processes such as nucleotide synthesis (**Fig 12**). Because it is known that *Acc2* deletion increases FAO and suppresses glucose utilization in the context of LV pressure overload, [29, 30] it is important to recall that cardiac myocytes within TG^{AC8} LV are smaller in size, and not enlarged as those in pathologic cardiac hypertrophy in response to LV pressure overload, [31] and in which ACC2 promotes glucose utilization and reduces FAO.[29, 30] In other terms, an increase in ACC2 appears to promote enhanced glucose utilization, enhanced aerobic glycolysis, enhanced utilization of the PPS, reduced FAO, and may be involved in the reduction of average LV cardiac myocyte size in TG^{AC8}, and the absence of markers of pathologic hypertrophy within the TG^{AC8} LV.

A Schematic of the Circuitry of Enhanced Cardiac Performance and Adaptive Mechanisms within the TG^{AC8} LV Derived from Phenotypic Characterization and Signals from Bioinformatic Analyses

Fig 13 depicts a hypothetical scheme of physiologic performance and protection circuits that appeared to be concurrently engaged within the TG^{AC8} LV. Because many of the perspectives depicted in the scheme in **Fig 13** were derived from bioinformatic analyses of cell lysates, it is not implied that all of these circuits are present within the same cell types that reside in the heart (see Discussion). Although the pathways/specific targets and the effector functions/outcomes culminating from the regulation of the components within the circuits in the pathways are represented according to published literature with respect to cardiac-specific context. The circuits (**Fig 13**) are based upon defined LV phenotypic characteristics (**Figs 1 - 9**, **Fig S.1, S2, S.9** and **Table S.1**), on signals derived from genotypic differences in transcriptome and proteome and IPA analyses (**Figs 10** and **11, Tables S.2-S.6**), on selected WB, RT-qPCR and immunolabeling analyses performed prior to and following transcriptome and proteome bioinformatic analyses, and

WB analyses (**Figs 2, 4-6, 8, S.10, S.15**), and on additional selected post-hoc WB, RT-qPCR (**Fig S.8-S.12**), performed having visualized the consilience of pathways depicted within the circuit schematic in **Fig 13**.

Discussion

Cardiac Structure and Contractile Performance Circuitry.

Because it is well known that alterations in heart structure and increased performance in the TG^{AC8} vs WT measured in vivo (**Fig 1 and S.1, Table S1)** and depicted in the scheme in **Fig 13** (left) can result from enhanced cAMP/PKA/Ca^{2+} signaling, we may conclude that the marked increases in AC8 protein level and activity and in PKA expression and activity in TG^{AC8} directly or indirectly lead to the differences in LV structure and performance in TG^{AC8} vs WT (**Fig 4 A-F**).

Left ventricular structure.

Although the TG^{AC8} LV wall thickness was increased, neither LV mass assessed via echocardiograms nor post-mortem LV weight, differed from WT (**Fig 1**), because the thicker LV walls in TG^{AC8} encompassed an LV cavity size that was markedly reduced at both end-diastole and end-systole compared to WT. Thus, because left ventricular hypertrophy, is strictly defined as an increase in LV mass, [17,18] the TG^{AC8} LV is not technically hypertrophied. Furthermore, pathologic hypertrophy markers were not increased in TG^{AC8}. It's of interest, however, that KO of, Protein Tyrosine Phosphatase Non-Receptor Type 1 (PTP1B AKA PTPN1), which protects against pathologic hypertrophy and increase in fetal gene markers in response to transverse aortic constriction[32] was increased by 2.5-fold in RNSEQ and 25% in proteome (**Table S.3, S.5**). Interestingly, although CITED4 was increased in in TG^{AC8} by WB, as would be expected in

response to chronic endurance exercise CEBPB transcript and protein were also increased in TG^{AC8} LV, directionally opposite of what occurs in the response to chronic exercise. [33]

The lack of an increase in LV mass in TG^{AC8} may be attributable, in part, to reduced LV wall stress (diastolic stretch), due to reduced filling volume, in TG^{AC8} vs WT, linked to the reduction in diastolic filling time, on the bases of the increased heart rate. Of note in this regard, the left atrial size was not enlarged in TG^{AC8} vs WT.

Histologic analysis of the thickened TG^{AC8} LV posterior wall revealed a cardiac myocyte profile that was shifted to cells that were smaller in size than WT (**Fig 2**). Thus, an increased density (per unit area) of smaller cardiac myocytes contributed to the increase in LV posterior wall thickness in TG^{AC8}. The LV wall collagen fraction did not differ by genotype (**Fig S2**), even though TGF β protein, TGF β receptor, and downstream signaling molecules were all upregulated (**Fig 13**). This suggests that additional adaptations that uncouple TGF β signaling from its effect increase fibrosis may become activated at this age in TG^{AC8} LV.

Left Ventricular Contractile Performance

Neither the early, nor the late diastolic filling rates, or early/late ratio differed by genotype (**Table S.1**), indicating that the smaller LV EDV in TG^{AC8} vs WT was not associated with reduced diastolic functional measures. LV myocardial contractility was markedly increased in TG^{AC8} vs WT as evidenced by markedly increased EF *in vivo* (**Fig 1**), as previously reported.[10] A 30% increase cardiac output in TG^{AC8} vs WT is attributable to the 30% increase in heart rate, because stroke volume did not differ by genotype (**Fig 1**).

As expected, expression of proteins that underly numerous cellular mechanisms driven by PKA signaling that determine cardiac myocyte contractile performance, were also upregulated in

the transcriptome (**Table S.3**), proteome (**Table S.5**) or in both transcriptome and proteome **(Fig S.5**, **Table S.7**) or in WB analyses (**Fig 4 G-J**) in TG^{AC8} vs WT. Both KCNJ2 and KCNQ1 K^+ channels which modulate cardiomyocyte membrane potential and action potential characteristics were upregulated in TG^{AC8} vs WT (**Fig 11**): KCNQ1 transcripts increased by 2.3-fold and protein increased by 26%; KCNJ2 transcripts increased by 3.2-fold and protein 32% (**Tables S.3, S5**). Of note, KCNJ2 regulation is mechanical sensitive and its increase in TG^{AC8} likely relates, at least in part, to the hypercontractile state of the TG^{AC8} LV.

It bears emphasis that the cardiac structural and resting performance profiles of the TG^{AC8} LV (**Fig 1**), therefore differ from those, observed in LV remodeling induced by chronic exercise endurance training, in which the diastolic cavity size, and stroke volume are increased at rest, [34] resting HR is reduced and cardiac output is unchanged. The cardiac myocyte profile in TG^{AC8} also differs from that induced in chronic exercise in which the LV myocytes size are increased but the myocyte number is unchanged.[35] The marked differences in cardiac structure and function between TG^{AC8} and the endurance-trained heart, in large part, likely to be attributable to increased vagal tone at rest in the latter, but not in the former,[8] in which an exercise functional profile is maintained around the clock at rest. In other terms the TG^{AC8} heart does not have an opportunity to rest between bouts of dynamic exercise as do the hearts of endurance trained organisms.

Cell Cycle, Proliferation, and Growth and Developmental Circuits

PKA signaling links many pathways involved in protein synthesis, (**Fig 11**) which was increased in the TG^{AC8} vs WT LV (**Fig 5A)**. Regulation of the synthesis of numerous proteins related to cell cycle, cell proliferation, and growth and development were increased in TG^{AC8} (**Tables S.3, S.5, S.10**). For example, the *Mras* oncogene transcript increased by 40%, and as noted, RAS protein was increased by 40% in TG^{AC8} vs WT (**Fig 5 B)**. Numerous molecules

downstream of RAS were increased and activated in TG^{AC8} LV including: RAF, MEK1/2 and ERK1/2 **(Fig 5 B, C**), indicating that MEK/ERK signaling, associated with enhanced cardiac proliferation[36] is activated to a greater extent in TG^{AC8} compared to WT (**Fig 13**, ERK arm).

AKT2 protein level and phosphorylation state were markedly increased in TG^{AC8} vs WT (see WB in **Fig S.8 A**). Numerous growth factor signaling molecules upstream of AKT were upregulated in TG^{AC8} vs WT (**Fig S.8, Figs 12, 13**) including periostin, which was increased by more than 100% in the transcriptome, and by 39% in proteome **(Tables S.10)** and by antibody array (**Fig S.14**). Of note, periostin plays a role in tissue regeneration, including wound healing, and ventricular remodeling following myocardial infarction. [37-39] *Egfr*, *Hdgf*, and *Igf1* transcripts were also increased in TG^{AC8}, and IGF1R protein was also borderline increased (**Table S.10).** Interestingly, some features of endurance exercise conditioning involve upregulation of IGF signaling via PIK3CA.[40] PIK3CA expression was increased in TG^{AC8} **(Fig S.7 A)**, as well as IGF signaling (**Table S.6A, B**).

Other molecules related to cell cycle, cell proliferation and growth and development that were increased in TG^{AC8} vs WT included: CDK2 (increased by 19%), CDK6 (increased by 36%), NOTCH1 (increased by 12%), beta1 catenin protein (increased by 17%), and PCNA (increased by 12%), *Hand2* (increased by 100%), and *Tbx5* and *Tbx20* transcripts both increased by 30% **(Table S.10)**.

Nuclear EdU labeling in cardiac myocytes did not differ by genotype. EdU labeling of non-cardiac myocytes, however, was substantially increased (**Fig 3**) in TG^{AC8} vs WT. Leading candidates of this regenerating cell network include endothelial cells, fibroblasts, immune cells, pericytes and most importantly, telocytes.[41]

Shifts in Metabolism

A greater **rate** of energy production in TG^{AC8} vs WT may be required to support, not only the higher HR and increased contractility during each heartbeat compared to WT, but also increased growth factor and other PI3K-directed signaling pathways, e.g. autophagy, protein synthesis and protein quality control (**Figs 5, 6, 13**).

The increased "energy requirements" of the TG^{AC8} LV are apparently being fully met because there is no indication that the TG^{AC8} LV is chronically hypoxic, as HIF-1α transcripts are down regulated (**Table S.2**) and HIF-1α protein level is reduced (**Fig S.8 B**). Further, steady levels of ATP and phosphocreatine in the WT LV *in vivo* at rest did not differ in TG^{AC8} vs WT (**Fig 9**). A prior study, in fact, indicates that exercise capacity of TG^{AC8} exceeds that of WT. [42]

Bioinformatic signals suggested that catabolism of glucose is markedly increased in TG^{AC8} vs WT (**Fig 12**). Enhancement of myocardial glucose catabolism was suggested by increases in GLUT1 (AKA Slc2a1) HK1 and PFK in TG^{AC8} vs WT LV (**Fig 11**). Of note, GLUT1 is the embryonic type of glucose transporter; [43, 44] and not the canonical heart form, GLUT4 (AKA Slc2a4) observed in the adult heart in response to myocardial stress.[45, 46]

Phosphorylation of GSK3B by AKT1 deactivates GSK3B. Inactivation of GSK3B via its phosphorylation is a key conversion point of a numerous processes that confer cardioprotection. [24] Although WB analysis indicated that GSK3B phosphorylation did not differ between genotypes, total GSK3B protein was significantly increased in TG^{AC8} vs WT (**Fig S.8 A**). Gys1 and phosphorylase kinase (PhK) were increased in the TG^{AC8} vs WT both the transcriptome and proteome (**Tables S.3 and S.5**) suggesting that a high turnover (increased synthesis and increased degradation) of glycogen may be involved in the marked increase in glucose catabolism within the

in TG^{AC8} LV (**Fig 12**). LV glycogen staining was modestly increased in the TG^{AC8} vs WT **(Fig S.13 B).**

Enhanced growth factor and other PI3K/AKT-driven signaling processes in TG^{AC8} suggested by omics analyses and validated in **Fig 12, 13, S.8, S.11** are tightly linked to ***aerobic glycolysis***.[28,47] It is well established that the **rate** at which ATP is generated in aerobic glycolysis is *greater* than that generated in oxidative phosphorylation via the TCA cycle and respiration.[28]

Bioinformatic analyses also indicated that in addition to increased expression of the glucose transporter, lactic acid dehydrogenase type A and the glutamine transporter, which are required for ***aerobic glycolysis***[28] are also increased in TG^{AC8} vs WT (**Figs 12, S.9**), suggesting that, relative to WT, the TG^{AC8} heart may utilize ***aerobic glycolysis*** to fulfill part of its energy needs. This idea is underscored by the absence of an increase in HIF1α (**Fig S.11 B**), suggesting the absence of hypoxia in the TG^{AC8} LV.[48, 49]

Aerobic glycolysis promotes utilization of the pentose phosphate shunt (PPS). PPS activation facilitates amino acid and nucleotide synthesis. Overexpression in TG^{AC8} LV of genes and proteins that are operative within the glucose metabolic pathway, e.g. G6PDH, PGD and PRPS2. (**Figs 12, S.8 C**), suggests that the PPS is more highly utilized in the TG^{AC8} vs WT LV.

Enhanced utilization of PPS in TG^{AC8} may be involved in re-synthesis of crucial amino acids and nucleotides following their degradation, (via increased autophagy, mitophagy and proteosome activity in TG^{AC8} vs WT, **Fig 6 D, G, I, J)**. PPS and may also be involved in catalyzing the replenishment of NADPH in TG^{AC8} via LDH and increased G6PDH and PGD (**Fig 12**), further ACLY, which catalyzes the **synthesis** of fatty acids (FA), leading to the formation of AcCoA, linking to synthesis of FA, lipids, phospholipids, and ceramides, was increased in TG^{AC8} vs WT

proteome analysis (**Figs 12, S.7, Table S.5**). Enhancement of these processes in TG^{AC8} via increased utilization of PPS may be linked to signals pointing to increased cell cycle, cell proliferation and growth and development in TG^{AC8} vs WT. In this context aerobic glycolysis and increased utilization of PPS in TG^{AC8} resembles heart **embryonic** differentiation and growth prior to the onset of the fetal stage when respiratory enzymes, e.g., COX7 are induced.[50] Thus, increased utilization of the PPS, in TG^{AC8} may be a crucial factor that underlies to promote increased cardiac biomass (increased number of small myocytes in LV wall, increased number of EdU-labeled nuclei, and increased LV wall thickness in TG^{AC8} vs WT **(Fig 1 and 2)** in the absence of increased collagen deposition (**Fig. S.2**)).

Bioinformatic signals suggested that the fatty acid β oxidation pathway and pathways that degrade branched chained amino acids are concurrently reduced, possibly due to reductions in CPT1, CPT2, ACAT1, HADH, HADHA, and HADHB (**Fig 12**). Bioinformatic analyses also suggested that utilization of TCA cycle and mitochondrial respiration within the TG^{AC8} LV are reduced compared to WT, even though the mitochondrial number and volume do not differ by genotype (**Fig 7 G, H**).

Downregulation of transcripts or proteins operative within the MAS, (*Ldhb, Mpc1, Mpc2, Mdh1, Got1, Slc25a11 Slc25a13,* and SLC25A13) **Fig 12 and Fig S.9** suggested that in conjunction with reduced TCA cycle and mitochondrial respiration in TG^{AC8} vs WT the translocation of H+ from cytosol to mitochondria to restore the level of mitochondrial NADH is also reduced in TG^{AC8}. An interaction between cytosolic lactate and the MAS has been proposed: cytosolic lactate formed during glycolysis may be used as a mitochondrial energy source via translocation of lactate via lactate-MAS within the same cell. Lactate can also be exported from one cell and taken up by other cells. [51] Under conditions when shuttling of NADH from cytosol

into the mitochondria via the MAS is limited, an increase in cytosolic lactate concentration might be expected to favor cytosolic NAD^+ regeneration via the LDH reaction. [52, 53] Thus, it might be expected that persistent high cardiac workloads that are characteristic of TG^{AC8} heart, in conjunction with reduced MAS and reduced expression of proteins involved in TCA cycle and mitochondrial respiration in TG^{AC8} vs WT, are associated with increased replenishment of cytosolic NADH from NAD+, at the expense of replenishment of mitochondrial NADH from NAD^+ within mitochondria. It is important to note that both transcripts and protein levels of IDH, which catalyze the oxidative decarboxylation of isocitrate to α-ketoglutarate, are reduced in TG^{AC8} vs WT, because during high cardiac workloads, as in the TG^{AC8} heart, the α-ketoglutarate/malate transporter located within the inner mitochondrial membrane does not compete favorably with mitochondrial matrix α-ketoglutarate dehydrogenase for α-ketoglutarate their common substrate.[53] It is well known that even in the presence of adequate oxygen during strenuous exercise requiring increased energy utilization, plasma lactate concentration becomes increased, suggesting that cytosolic lactate is increased[54] in the TG^{AC8} heart, favoring NAD^+ regeneration in the cytosol. [55]

ROS Regulation

Although increased rates and amounts of ATP production and utilization in the TG^{AC8} heart to support simultaneous increased cardiac performance and growth factor signaling are likely to be associated with a substantial increase in ROS generation, ROS levels were not increased in the TG^{AC8} LV (**Fig 8 B**). Because ATP production via aerobic glycolysis generates less ROS compared respiration,[28] increased utilization of aerobic glycolysis would be one mechanism to limit ROS production within the TG^{AC8} LV. Other mechanisms to reduce ROS levels that appeared to be utilized to the greater extent in TG^{AC8} vs WT include NRF2 signaling, one of the top enriched and activated pathways **(Figs 8 A, 10 C),** SOD3 (transcripts increased by 3.2-fold and protein by 20%),

and HMOX1 (transcripts increased by 54% and protein by 32%; **Table S.7**) which not only protects tissue against oxidative stress, but also protects against apoptosis.[56, 57] HMOX1 is an important activator of NRF1, which has been recently discovered to be involved in heart regeneration and repair, promoted by NRF1 signaling.[58] Importantly, four members of the family of glutathione peroxidases involved in the termination reaction of ROS pathways were increased in TG^{AC8} vs WT: Gpx3 (transcripts by 103%, proteins by 30%); Gpx7 (transcripts by 40%, proteins by 21%); Gpx8 (transcripts by 20%, proteins by 16%); Gpx1 (transcripts by 39%, proteins by 12%). Several members of glutathione transferases were differentially expressed in TG^{AC8} vs WT: Gsta3 (transcripts and proteins upregulated by 55% and 26% respectively); GSTM5 (proteins upregulated by 23%), GSTM1 (proteins upregulated by 14%); mitochondrial glutathione reductase GSR was also upregulated, while GSTM7 (transcripts and proteins were decreased by 21%, and 9%) and GSTO1 (protein was decreased by 9%).

Cardiac Protection Circuitry

Negative feedback on βAR-cAMP-PKA-Ca signaling

Numerous molecules that **inhibit** βAR signaling, (e.g. Grk5 by 2.6 fold in RNASEQ and 30% in proteome; Dab2 by 1.14 fold in RNASEQ and 18% in proteome; and β-arrestin by 1.2 fold in RNASEQ and 14% in proteome) were upregulated in the TG^{AC8} vs WT LV (**Table S.3, S.5** and **S.9)**, suggesting that βAR signaling is downregulated in TG^{AC8} vs WT, and prior studies indicate that βAR stimulation-induced contractile and HR responses are blunted in TG^{AC8} vs WT.[8,11] The heart, itself, produces catecholamines, (**Fig S.3 A**). It is interesting to note that βARs become desensitized in TG^{AC8} (**Fig S.3 B**), even though neither plasma norepinephrine, nor epinephrine are increased, but reduced in TG^{AC8} vs WT[8] (**Fig S.3 C**).

Both the RNASEQ and proteome analyses indicated that PI3K/AKT signaling, which promotes survival,[59] is activated in TG^{AC8} vs WT (**Fig 11** and **13**). Numerous studies have indicated that PI3K signaling is involved in βAR internalization,[60,61] and is also involved in cAMP metabolism by acting as an essential component of a complex controlling PDE3B phosphodiesterase-mediated cAMP destruction.[62,63]

In cultured cardiomyocytes, βAR stimulation increases PI3K activity.[64, 65] Both the β1AR and β2AR have been reported to transactivate PI3K in vitro.[66, 67] Moreover, βAR stimulation-induced increases in heart weight, contractile abnormalities, and myocardial fibrosis, and cardiac "fetal" genes were markedly attenuated in the absence of PI3K expression.[68] Although this formidable evidence in most cases has identified PI3Kγ to be specifically involved in cardioprotection with response to G-protein coupled receptor signaling, PI3Kγ was not identified in our transcriptome or proteome analyses, but RT-qPCR assay detected significant increase of catalytic subunit of PI3Kγ (*Pi3kcg)* expression (**Table S.9**). Tyrosine receptor coupled PI3KCA, AKT and PDK1 were increased in TG^{AC8} vs WT proteome, and these proteins, as well as PTEN (WB) and PIP3 (ELISA) were increased TG^{AC8} vs WT (**Fig 12, Fig S.7**).

A blunted response to βAR stimulation in a prior report was linked to a smaller increase in L-type Ca^{2+} channel current in response to βAR stimulation in the context of increased PDE activity.[13, 14] WB analyses showed that PDE3A and PDE4A expression increased by 94% and 36%, respectively in TG^{AC8} vs WT, whereas PDE4B and PDE4D did not differ statistically by genotype (**Fig S.11 A**). In addition to mechanisms that limit cAMP signaling, the expression of endogenous PKI-inhibitor protein (PKIA), which limits signaling of downstream of PKA was increased by 93% ($p<0.001$) in TG^{AC8} vs WT (**Table S.3**). Protein phosphatase 1 (PP1) was increased by 50% (**Fig S.11 A**). The Dopamine-DARPP-32 feedback on cAMP signaling pathway was enriched and

also activated in TG^{AC8} vs WT (**Fig 12**), the LV and plasma levels of dopamine were increased, and DARPP-32 protein was increased in WB by 269% (**Fig S.11 A**).

Thus, mechanisms that limit signaling downstream of AC-PKA signaling (βAR desensitization, increased PDEs, PKI inhibitor protein, and phosphoprotein phosphatases, and increased DARPP-32, cAMP (dopamine- and cAMP-regulated phosphoprotein)) are crucial components of the cardio-protection circuit that emerge in response to chronic and marked increases in AC and PKA activities (**Fig 4 C, F**).

Upregulation of stress response pathways.

Beyond the adaptations to limit the degree to which cAMP/PKA signaling is activated, numerous canonical stress-response signaling circuits were concurrently enriched in TG^{AC8} (**Fig 13**). Multiple parallel cascades of stress response receptor signaling within circuits downstream of AC signaling (**Fig 13)**, include: RTKs (PI3K/AKT, ERK-MAPK); cytokine receptors (JNK1/2, JAK2/STAT3), pattern recognition receptor RAGE (S100/calgranulins) and T-cell receptor (NF-κB) (**Fig 13**). The main functional category of genotypic changes identified in PROTEOMAP analysis, **Environmental Information Processing** (**Figure S.7**), points to an integration of these stress response pathways. The consilience of cardio-protective adaptations that result from integrated activation of signaling cascades that were enriched in TG^{AC8} included: cell survival initiation, protection from apoptosis, proliferation, prevention of cardiac-myocyte hypertrophy, increased protein synthesis and quality control, increased inflammatory and immune responses, facilitation of tissue damage repair and regeneration and increased aerobic energetics (**Fig 13**).

Pathways downstream of receptor tyrosine kinase (RTK), a classical cognate receptor, amongst others, transmits signals to promote the activation of PI3 kinase and RAS-RAF-MEK1/2-

ERK1/2 (**Fig 13**). Receptor activation by adrenergic agonists and growth factors (such as periostin, increased by 39% in omics and validated by antibody array (**Table S.5, Fig S.14**) bind to β-AR and RTK, respectively. Ras-p21 functions as a molecular link for membrane GPCR and RTK to transduce signals from these receptors to downstream signaling machinery (**Figure 13**, ERK arm). Ras-Raf-MEK-ERK pathway plays a key role in cardioprotection in the context of ischemia-reperfusion injury and oxidative stress.[69] Downstream of Ras-p21, c-Raf is subsequently induced, which, in turn, sequentially activates MEK1/2 and ERK1/2 to achieve their downstream effects (**Fig 13**, ERK arm, **Fig 4 B, C**). MEK/ERK1/2 activation promotes tissue repair that is essential for repair of damaged cells or cell regeneration (see below) in response to cardiac stress in vivo (**Figure 13**, ERK arm), especially those observed in genetically engineered animal models.[70]

Ras-p21 signaling also exerts protective influences on cell reparative and regenerative capacity, presumably via activation of ERK-independent downstream pathways of PI3K/AKT signaling[71, 36]. Increased expression of the catalytic subunit PIK3CA in TG^{AC8} by 15 % in WB (**Fig. S.8 A**) may be linked to the activation of the downstream targets, including PDK1 phosphorylation on serine 241, subsequent phosphorylation of AKT2 (i.e., threonine 308 and serine 473) and of the transcription factor, Foxo1, at serine 256 (**Fig S.11 B, Figure 13**, PI3K arm, bottom panel). Activation of AKT inhibits hypertrophic signaling in adult hearts in vivo, [72 73 74 18] while inducing protein synthesis and activating protein quality control signaling [75] (**Figure 13**, PI3K arm). This anti-hypertrophic effect of AKT in TG^{AC8} may be linked to the lack of increased myocyte size and absence of increased LV mass in TG^{AC8} (**Figs 1J, 2B, C, D**), (see below), even in the presence of elevated α-skeletal-actin and MYH6 (**Fig 4 G, Figure 13,** bottom panel).

The tumor suppressor PTEN is a lipid phosphatase that regulates cell growth, survival and migration by catalyzing the dephosphorylation of the phospholipid phosphatidylinositol (3,4,5)-

trisphosphate PtdIns (3,4,5)P3 or PIP3, an integral second messenger molecule for the PI3K-AKT signaling, thus antagonizing this pathway. PTEN protein abundance was increased by approximately 28% ($p<0.01$) in the TG^{AC8} LV compared to WT by WB (**Fig S.8 E**), in concordance with proteomics data, which showed a 22% increase in PTEN ($p=0.053$) in the TG^{AC8} LV. Phosphorylation of sites within the PTEN C-terminal domain, including S380, T382 and T383, have been demonstrated to be involved in the regulation of stability and activity, with a loss in phosphorylation leading to membrane recruitment and greater activity followed by rapid proteosome-mediated degradation.[76,77,78] Phosphorylation of Ser380 residues was significantly lower in TG^{AC8} vs WT (-35%, $p<0.05$) as was the ratio of p-PTEN Ser380/Total PTEN (-50.15%, $p<0.005$) (**Fig S.8**), suggesting that PTEN activity is increased in the TG^{AC8} vs WT. A 2-fold higher expression of PIP3 in TG^{AC8} vs WT, determined by ELISA, along with increases in PI3K catalytic subunit abundance and AKT activity, strongly suggest that PTEN does not exert **a net** negative regulatory effect in TG^{AC8} on this pathway. Rather, an increase in PTEN in TG^{AC8} may be necessary to maintain the available pool of PIP2 that is required for phospholipid metabolism, and other signaling pathways, such as e.g. PLC/IP3/DAG signaling (important in Ca^{2+} regulation), or in functional processes like e.g. Endocytosis and Actin cytoskeleton remodeling,[79] that are enriched and activated in TG^{AC8} vs WT (**Fig 10 C and Table S.6 A,B**).

Integral components of the PI3K-AKT and RAS-RAF-MEK1/2-ERK1/2 survival-associated pathways converge to suppress apoptosis[80,81,82] (**Figure 13**, PI3K and ERK arms). Caspase-3 levels were increased (**Fig S.11 B**). The barely detectable or low protein expression of hallmarks of apoptosis in TG^{AC8} LV, including *cleaved* caspase-3 and its downstream *cleaved* PARPs, suggest that apoptosis suppression signaling mechanisms become activated in the TG^{AC8} LV (**Fig S.11 B and Fig 13**, PI3K and ERK arms top and bottom panels). That full-length caspase-

3 expression was increased in TG^{AC8} vs WT, but not cleaved (**Fig S.11 B and Fig 12**),[83] provides strong evidence of activation anti-apoptotic functions of caspase-3 activation in the TG^{AC8} LV. Further, there was no indication of increased apoptotic nuclei in TG^{AC8} LV tissue (**Fig S.13 A**).

Proteostasis

Many upregulated transcripts and proteins in TG^{AC8} vs WT (**Fig S.7, Tables S3, S.5**), including the serine/threonine-protein kinases, MSK1 and MNK1, might signal within cardio-protective pathways (**Figs 5 F, G; 13**). Specifically, MSK1 is involved in regulation of the transcription factors CREB1, ATF1, RELA and STAT3. MNK1 is involved in the initiation of protein translation by interacting with eIF4G and phosphorylating eIF4E.

The Small Proline Rich Protein 1 **Sprr1a,** which is linked to induction of protein synthesis (**Figure 13**, bottom panel), was the most abundantly overexpressed transcript **and** protein in the TG^{AC8} **LV (Table S.7 A).** Immunolabeling of Sprr1a in single LV myocytes isolated from TG^{AC8} is illustrated in **Fig S.15**. Sprr1a is associated with inflammation, cellular stress, and repair[84,85] and has been linked to protection against cardiomyocyte death in the setting of ischemia–reperfusion injury.[86,87] Sprr1a stimulates the expression of Rtn4 (**Fig S.15**), a member of the reticulon encoding gene family associated with endoplasmic reticulum that is involved in neuroendocrine secretion or in membrane trafficking in neuroendocrine cells.[88, 89] Rtn4, which was also overexpressed in TG^{AC8} vs WT (transcripts increased by 50% and proteins increased by 30%, **Fig** S.**15**, **Table S.7 A)**.

Derlin1, a protein that was also markedly overexpressed in TG^{AC8} vs WT (by 132%, **Table S.5**) participates in the ER associated protein degradation by recognizing and selecting misfolded or unfolded proteins and translocating these from the ER lumen to the cytosol for proteasomal

degradation. Calnexin, and calreticulin both members of the CALR/CN cycle, which ensures the quality and folding of newly synthesized molecules within the endoplasmic reticulum, were also both increased by WB in TG^{AC8} (**Fig S.11 D**). Numerous other molecules involved in unfolded protein response signaling significantly differed by genotype in omics analyses: transcripts included ATF4, ATF6, Caspase 3, CALR, HSP90 (**Table S.3**); proteins included: CASP3, CASP6, HSP90α (**Table S.5**).

Autophagy

Forced changes in energy metabolism, downstream of markedly increased levels of AC/cAMP/PKA signaling in TG^{AC8}, and resultant adaptations to this stress (**Fig 13)**, may produce excess wear-and-tear damage in cellular components, requiring an adaptively higher autophagy/mitophagy machinery. The preserved level of mitochondrial fitness (**Fig 6 I, J; Fig 7 M, N**) in TG^{AC8}, in the context of marked chronic AC-driven cellular stress, likely reflects one such autophagic adaptation. Protein levels of ATG13, ATG4B and PARKIN, members of the autophagy machinery were upregulated in TG^{AC8} vs WT (**Fig 6 E-G**). Specifically, the cysteine protease ATG4B processes pro-MAP1LC3 and pro-GABARAP in the early stages of autophagy and endocytosis pathways, before their lipidation (addition of the phosphatidylethanolamine) by ATG7 and ATG3. Being also involved in MAP1LC3/GABARAP delipidation, it plays a key role in their turnover. The autophagy-related protein ATG13 is a factor required for autophagosome formation and part of the initiation complex with ULK1 and RB1CC1. It is also involved in mitophagy, together with the E3 ubiquitin-protein ligase PARKIN, which acts downstream of PINK1. Upregulation of these proteins protects against mitochondrial dysfunction during cellular stress by coordinating mitochondrial quality control mechanisms that remove and replace dysfunctional mitochondrial components.

Inflammation/Immune Signaling.

The myocardium is intimately connected with the immune system and activation of the immune system has been shown to have both protective and maladaptive effects on the heart. [90] This inherent duality of the immune system has spurred a quest for tools to harvest the protective effect of the innate and adaptive immune response without experiencing their detrimental effects. [91] On this background, it is remarkable that the most upregulated pathway in the TG^{AC8} hearts was "leukocyte extravasation signaling" (**Fig 10 C**) and that the TG^{AC8} was characterized by up regulation of several inflammatory molecules and pathways, both in the "omics analysis" and in western blot based or RT-qPCR based validation analyses. TG^{AC8} hearts in fact showed upregulation of *IL-6*, *IL-10*, ICAM1, and CCL12 (**validated in Fig S.12 A**). Furthermore, they showed upregulation of MAGUK and MALT1 of the CBM complex together with its downstream NF-κB signaling (NF-κB coactivators TRAF2/6 and ATF3 (**Fig 13,** NF-κB arm, **Fig S.7**, **Table S3, S.5 and Fig S.12 A**)). The TG^{AC8} heart was also characterized by phosphorylation of JNK1/2 on threonine 183 and tyrosine 185 (**Fig 13**, JNK arm, and **Fig S.8**) that paralleled gene expression changes consistent with activation of the JNK1/2 signaling pathway in TG^{AC8} vs WT (**Tables S.3, S.5, S.6 B**).

The fact that we detected upregulation of T cell receptor signaling and B cell receptor signaling (**Table S.6 A, B**) together with the fact that we detected upregulation of the CBM complex (central in B and T cell activation) suggests that the AC8 heart might be characterized by recruitment of T and B cells to the myocardium. [92] Specific subclasses of lymphocytes have been shown to have protective effect on the heart. [90] JNK1/2 activation is centrally involved in inflammatory signaling[93] but also linked to inhibition of cardiac hypertrophy[94] and promotion of reparative and regenerative capacities. [95] Taken together, these observations raise the intriguing

possibility that the AC8 overexpressing heart might manage to cope with continuous stress also through the activation of a cardio-protective immune responses.

TG^{AC8} LV protection circuits resemble some adaptive mechanisms that accompany disease states.

We next performed IPA analyses in order to ascertain the extent to which cardiac protection circuits identified in the TG^{AC8} LV (**Fig 13**) might be utilized as adaptations to the stress of various disease states. The top disease categories identified in both the TG^{AC8} transcriptome and proteome were **Organismal Injury and Abnormalities and Cancer (Fig S.16),** the latter being subsumed within the former category. This is not surprising, because the sequalae of marked chronically increased AC/cAMP/PKA signaling illustrated in TG^{AC8} LV protection circuitry **(Fig 13),** are very similar to the "**Hallmarks of Cancer**",[15, 16] and included: protection from apoptosis, survival, aerobic glycolysis, increased proliferation, enhanced protein synthesis and quality control, increased inflammatory and immune response, enhanced tissue damage repair and regeneration. Thus, the TG^{AC8} LV utilizes a consilient pattern of adaptive mechanisms that emerge in many cancer cell types for self-protection.[15,16] The altered cancer-like protection circuitry manifested within the TG^{AC8} LV most resembles that of gliomas,[96] and in this regard three distinct IPA signaling pathways (Glioblastoma Multiforme Signaling, Glioma Invasiveness Signaling, Glioma Signaling (**Table S.6 A,B)**) were highly enriched and activated in TG^{AC8} vs WT. This protection circuitry allows the adult TG^{AC8} heart to cope (for at least up to a year),[10] with numerous, marked cell-tissue stressors driven by the markedly augmented AC-cAMP-PKA-Ca^{2+} signaling. "Limited versions" of this cardio-protective profile that emerges within TG^{AC8} LV have also been previously discovered to be central to cardiac ischemic pre-conditioning[97] and exercise endurance cardiac conditioning.[1,98]

Opportunities for Future Scientific Inquiry Afforded by the Present Results

By design our systems approach to elucidate some general foundations of the consilient adaptation profile that protects the chronically high performing TG^{AC8} heart, represents only a "first port of call", defining some general features of the TG^{AC8} cardiac performance/protection profile. Because many of the perspectives depicted in the scheme in **Fig 13** were derived from bioinformatic analyses of cell lysates, it is not implied that all of these circuits are present or become activated in all cell types that reside in the LV myocardium. It is apparent, however, from our results, consilient shifts in enrichment or activation of numerous stress response pathways accrue to allow for the chronic high-level performance of the TG^{AC8} LV. Similarly, a consilience of shifts in numerous stress response pathways may be of biological significance in pathologic states, for example, e.g. consilient adaptations may be allowed for proper healing in disease state, e.g. myocardial infarction or chronic heart failure.

A most important aspect of our results, is that they identify numerous hypotheses that can be tested in future, more in depth studies aimed at: (1) defining the precise cardiac cell types in which protection circuitry is activated in the chronically over-worked TG^{AC8} heart; (2) providing deeper definitions of the multitude of signaling pathways that differed significantly in enrichment and activation status among cell types in TG^{AC8} vs WT (**Figs 10-13, Table S.6 A, B**). This will lead to identification of novel associations among the concurrently activated adaptive mechanisms within and among cell types in TG^{AC8} LV that are not intuitively linked to cardiac protection in the context of our current state of knowledge. For example, elucidation of specific details within the leukocyte extravasation pathway, the top activated IPA canonical pathway in TG^{AC8}, and of other highly activated canonical signaling pathways in TG^{AC8} vs WT (**Fig 10 C** and **Table S.6 A, B)**, that are not usually addressed in the field of cardiac research. This will permit detection of

crosstalk between cardiac myocytes and other cell types such as immune cells and others that is likely to be critical to the cardiac protective and performance-enhancing circuitry that is harbored within TG^{AC8} heart (**Fig 13**). (3) Identification post-translational protein modifications e.g. via delineations of changes in the TG^{AC8} LV phosphoproteome, ubiquitome, acetylome, and 14-3-3 interactome; (4) identifying specific types of intersticial cells that proliferate within the LV myocardium that was predicted by our omics results, and validated by EdU and BrdU labeling of the young adult TG^{AC8} heart between 2 and 3 mo (**Fig 3**). (5) precisely defining shifts in metabolism within the cell types that comprise the TG^{AC8} LV myocardium via metabolomic analyses, including fluxomics.[99] It will be also important that future metabolomics studies elucidate post-translational modifications (e.g. phosphorylation, acetylation, ubiquitination and 14-3-3 binding) of specific metabolic enzymes of the TG^{AC8} LV, and how these modifications affect their enzymatic activity.

Finally, chronic consilient utilization of numerous adaptive pathways, however, may present a double-edged sword, compensating for chronic stress in the "short run", but becoming maladaptive when utilized over prolonged periods of time. In fact, TG^{AC8} mice have a reduced (about 30%),[10] a median life span, and later in life (at about 12 mo) marked LV fibrosis and dilated cardiomyopathy occur. Future studies are required to precisely discover how the consilience of cardio-protective adaptations harbored within the TG^{AC8} heart at 3 mo of age that were defined in present study fails over a protracted time-course are extremely important. It is noteworthy in this regard, when our omics data were specifically filtered for "**cardiovascular system"** and "**cardiovascular disease"** in bioinformatic analyses, features common to variety of cardiomyopathies were predicted in the "super-performing" TG^{AC8} LV (**Table S.11 A, B**). The basis of this prediction may stem from the fact that omics "knowledge" generated by findings in

prior cross-sectional studies of experimental heart failure, it seems to us may have often been misinterpreted to be **causal** factors of the heart failure, rather than adaptations that react to ameliorate the heart failure, due to a lack of longitudinal prospective. Thus studies, conducted *longitudinally* over the TG^{AC8} life course, to generate testable hypothesis about which of these correlated findings are *cause-and-effect* vs those that are simply *associated* are required to dissect out which factors that enable the "super performing heart" of the TG^{AC8} during young adulthood, gradually fail over a prolonged period of time, resulting not only in accelerated aging, but also in and frank, severe, dilated cardiomyopathy.[10]

Acknowledgments

We thank the NIDA Confocal and Electron Microscopy Core for access to their equipment, and specifically Zhang Shiliang (Core manager) and Marisela Morales (Director). We wish to thank Loretta Lakatta for her superb editorial assistance.

Funding

This research was supported by the Intramural Research Program of the NIH, National Institute on Aging (USA).

Figure Legends

Figure 1. (A-K), Echocardiographic parameters (N= 28 for TG^{AC8}; WT=21); L heart weight/body weight at sacrifice (N=75 for TG^{AC8} and N=85 for WT). See Table S.1 for additional Echo parameters.

Figure 2. (A) WB of Pathologic hypertrophy markers, *(B, C)* cardiac myocyte size and distributions of cardiac myocytes, (*D) Representative LV sections depicting cardiac myocyte diameters,*

Figure 3 (A-G) representative examples of confocal images (400x) of LV WGA (red), vimentin (Cyan), EdU (yellow), DAPI (blue), (H) average number of EdU labeled nuclei positive field counts in LV TG^{AC8} vs WT (N=3 mice in each genotype). Detection of cardiomyocyte S-phase activity. (I) Section from the heart of a TG^{AC8}, MHC-nLAC double-transgenic mouse subjected to 12 days of BrdU treatment. The section was processed for β-galactosidase (to identify cardiomyocyte nuclei, red signal) and BrdU (to identify DNA synthesis, green signal) immune reactivity, and then counterstained with Hoechst (which stains all nuclei, blue signal). (J) Example of an S-phase cardiomyocyte nucleus detected with this assay. The upper panel shows β-galactosidase immune reactivity (red channel), the middle panel shows BrdU immune reactivity (green channel), and the lower panel shows a red and green color combined image of the same field. The arrow identifies an S-phase cardiomyocyte nucleus, as evidenced by the overlay of β-galactosidase and BrdU immune reactivity, which appears yellow in the color combined image. (H) Graph representing S-phase activity in the TG^{AC8}, MHC-nLAC double-transgenic vs. the MHC-nLAC single transgenic animals (mean +/- SEM, p=0.315; 5 mice per genotype and 3 sections per mouse were analyzed).

Figure 4. (A) Representative examples of ADCY8 immunolabeling in TG^{AC8} and WT LV cardiomyocytes, **(B)** Average AC8 fluorescence in LV cardiomyocytes and **(C)** Average AC activity in TG^{AC8} vs WT, **(D, E)** Expression levels of PKA catalytic and regulatory subunits, and **(F)** PKA activity in TG^{AC8} vs WT, **(G-M)** Western Blot analysis of selected proteins involved in excitation - Ca release – contraction-relaxation coupling TG^{AC8} vs WT LV. **(L)** RyR2 immunolabeling. Antibodies employed are listed in supplemental methods. (N=199 WT cells and 195 TG^{AC8} cells (each from 3 mice)**.**

Figure 5. (A) Rate of global protein synthesis and **(B-G)** mechanisms downstream of PKA signaling involved in protein synthesis in the TG^{AC8} and WT**.**

Figure 6. (A) Proteosome activity assay and **(B, C)** accumulated proteins in soluble and insoluble fractions of LV lysates in TG^{AC8} vs WT. **(D)** WB of HSP90 in TG^{AC8} and WT, **(E-H)** Expression levels of selected proteins involved in the autophagy process. **(I, J)** Autophagolysosome accumulation is enhanced in AC8 mice. The statistical significance is indicated by **($p<0.01$) and t ($p<0.01$ in one-tailed t test).

Figure 7. (A, B) Representative panoramic electron micrographs and **(C-F)** higher resolution images of LV cardiac muscle fibers and mitochondria in TG^{AC8} and WT. White arrowheads depict lipid droplets; asterisks show swollen, disrupted mitochondria with lighter cristae compared to the surrounding, healthy mitochondria. **(G, H)** Average mitochondrial number of quantitative stereological analyses of normal mitochondrial number and volume, **(I, J)** damaged mitochondria**,** **(K, L)** number of lipid droplets per cell area and volume of lipid droplets. **(M, N)** mPTP-ROS threshold, measured in a single LV cardiac myocyte, did not differ between TG^{AC8} and WT mice. Insulin was employed as a positive control. (N=3 in each genotype) (** $p<0.01$, *** $p <0.001$)**.**

Figure 8 (A) WB analysis of Nrf2 expression in LV TGA^{C8} vs WT. (B) LV performance and the rate of superoxide (ROS) generation in isolated working TG^{AC8} and WT hearts.

Figure 9 (A) A schematic of ATP creatine energy system, (B) Representative $_{P}$31 NMR spectra of TGAC8 and WT hearts. (C-E) average levels of ATP, PCr, and ATP/PCr in TGAC8 and WT hearts derived from NMR spectra.

Figure 10 (A) Schematic of the total number of transcripts (subset "a" – 11,810), and proteins (subset "b" 6,834), identified in LV lysates, the number of transcripts (subset "d" 2,323), and proteins (subset "d" 2,184), that differed by genotype, and number of identified transcripts and proteins that both differed by genotype (subset "e" - 544). (B) WEBGESTALT analysis of the XX transcripts (Panel A subset "c") and YY proteins (Panel A subset "d") that significantly differed by genotype. Biological Processes (BP), Cell Compartment (CC), Molecular Functions (MF). (C) Top canonical signaling pathways differing in enrichment (-log(pvalue) >1.3) and activation status by genotype (Z-score: figure key) in IPA analysis of transcripts and proteins.

Figure 11 Regulatory Networks Centered on Adenylyl Cyclase and Protein Kinase A Signaling.

Gene families of proteins regulated by PKA ranged from transcription regulators, kinases, peptidases and other enzymes, transmembrane receptors, ion channels and other gene families. Canonical signaling pathways in which these proteins operate and downstream biological and molecular processes of proteins in these pathways are also displayed (lower part). See **Table S.8** for the full list of these downstream effects of PKA signaling.

Figure 12 Growth and Metabolism.

A schematic of growth and metabolism circuitry based on signals derived from bioinformatic analyses of the transcriptome and proteome and on selected WBs. Catabolism of glucose is

markedly increased in TG^{AC8} vs WT as reflected in increased expression of Glut1, HK1 and PFK and other glycolytic enzymes, whilst fatty acid β oxidation pathway is concurrently reduced, as reflected in reduced expression of Cpt1, Cpt2, Acat1, Hadh, Hadha, and Hadhb. in TG^{AC8} vs WT LV. Shifts in the transcription of genes and translation of proteins that are operative within PPS pathway, i.e. G6PDH, PGD and PRPS2 suggests that PPS is more highly activated in the TG^{AC8} vs WT. The combination of increased expression of the glucose transporter, lactic acid dehydrogenase type A and the glutamine transporter in TG^{AC8}, suggests that, relative to WT, the TG^{AC8} heart utilizes aerobic glycolysis to fulfill part of its energy needs. Enhanced growth factor and other PI3/AKT driven signaling processes increased in TG^{AC8} vs WT are also known to be linked to aerobic glycolysis.

Figure 13. Schematic of TG^{AC8} Heart Performance and Protection Circuits that appeared to be concurrently engaged in the TG^{AC8} LV.

The pathways/specific targets and the effector functions/outcomes culminating from the regulation of the components within the circuits in the pathways are represented according to published literature with respect to cardiac-specific context (See Discussion). **Pink colors** represent proteins that differed by genotype in WB. Molecular targets or components in **red**, **green,** and **grey** represent molecular targets or components that are increased or upregulated, decreased or downregulated, or unchanged, respectively, in TG^{AC8} vs WT.

Supplements

Supplemental Tables

Table S.1. List of Echo parameters recorded in TG^{AC8} heart vs WT.

Table S.2. A Listing of all 11810 identified transcripts.

Table S.3. A listing of 2323 transcripts that significantly differed in expression by genotype.

Table S.4. A listing of all 6834 identified proteins.

Table S.5 A listing of 2184 proteins that significantly differed in expression by genotype.

Table S.6. A listing of canonical pathways in IPA analysis of the total number of (A) transcripts and (B) proteins that were differentially enriched or activated in TG^{AC8} vs WT. (C) A listing of molecules with indication of involvement in number of pathways.

Table S.7. (A) A listing of 544 molecules of which both transcripts and proteins differed by genotype. (B) A listing of canonical pathways that were differentially enriched by genotype in IPA analysis of 544 transcripts and proteins.

Table S.8. A Complete list of downstream effects of enriched canonical signaling pathways in TG^{AC8}, depicted on Figure 11.

Table S.9. RT-qPCR analysis of selected transcripts related to G-protein Coupled Receptor Signaling, that differed by genotype in RNASEQ.

Table S.10 Transcripts and proteins involved in Cell Cycle/Cell Proliferation, and Growth and Developmental Circuits that differed between TG^{AC8} vs WT.

Table S.11 IPA representation of top cardiovascular disease-related functions within the LV (A) transcriptome and (B) proteome of TG^{AC8} and WT.

Table S.12 Primers used in RT-qPCR analyses

Table S.13 Antibodies used in WB analyses and antibody arrays

Supplemental Figures

Figure S.1 Representative images of echocardiograms.

Figure S.2 Representative LV sections, and average collagen density.

Figure S.3 Pathway for catecholamine synthesis and breakdown, myocardial and plasma catecholamine levels.

Figure S.4 Volcano plots and heat maps of transcripts and proteins.

Figure S.5. Spearman's correlations of Z-scores of IPA transcriptome and proteome canonical pathways that significantly differed by genotype.

Figure S6. Correlation plot of 544 identified molecules of which *both* transcripts and proteins differed by genotype.

Figure S.7. PROTEOMAP.

Figure S.8 WB analyses of Selected Proteins that mediate PIP3 Kinase Signaling and Metabolism.

Fig S.9 Detailed schematic malate-aspartate shuttle based on signals derived from bioinformatic analyses of the transcriptome and proteome and on selected WBs.

Figure S.10 Representative examples of (A) ACACB immunolabeling of TG^{AC8} and WT LV myocytes; (B) average ACACB fluorescence in LV cardiomyocytes (n=25 for each group); (C) Relative Quantification of Acaca mRNA expression in LV tissue (n=4 for each group).

Figure S.11 WB Analyses of Selected Proteins Within the Performance and Protection Circuitry Depicted in Fig 13. (A) Negative feedback adaptations on AC/PKA signaling, (B) WB analysis of selected proteins involved in Jak/Stat/Jnk/Caspase signaling. (C) WB analysis of selected proteins involved in angiotensin receptor signaling. (D) WB analysis of Calnexin and Calreticulin, proteins involved in ER protein processing.

Figure S.12 RT-qPCR analysis of genes regulating cytokines level in the LV genes and Cytokines levels measured from heart tissue lysates.

Figure S.13 LV Tissue Staining for apoptosis and Glycogen.

Figure S.14 Periostin levels detected in TG^{AC8} vs WT LV (Growth Factor Quantibody Array)

Figure S.15 Sprr1 signaling network, Immunolabeling of Sprr1a in isolated LV myocytes, and WB analysis of RTN4 expression.

Figure S.16. IPA representation of top Disease-related functions within the LV transcriptome and proteome of TG^{AC8} and WT.

References

1. Vega RB, Konhilas JP, Kelly DP and Leinwand LA. Molecular Mechanisms Underlying Cardiac Adaptation to Exercise. *Cell Metab*. 2017;25:1012-1026.
2. Ventura-Clapier R, Mettauer B and Bigard X. Beneficial effects of endurance training on cardiac and skeletal muscle energy metabolism in heart failure. *Cardiovasc Res*. 2007;73:10-8.
3. Lovallo WR. Cardiovascular reactivity: mechanisms and pathways to cardiovascular disease. *Int J Psychophysiol*. 2005;58:119-32.
4. Zhang X, Szeto C, Gao E, Tang M, Jin J, Fu Q, Makarewich C, Ai X, Li Y, Tang A, Wang J, Gao H, Wang F, Ge XJ, Kunapuli SP, Zhou L, Zeng C, Xiang KY and Chen X. Cardiotoxic and cardioprotective features of chronic beta-adrenergic signaling. *Circ Res*. 2013;112:498-509.
5. Antos CL, Frey N, Marx SO, Reiken S, Gaburjakova M, Richardson JA, Marks AR and Olson EN. Dilated cardiomyopathy and sudden death resulting from constitutive activation of protein kinase a. *Circ Res*. 2001;89:997-1004.
6. Squire IB and Barnett DB. The rational use of beta-adrenoceptor blockers in the treatment of heart failure. The changing face of an old therapy. *Br J Clin Pharmacol*. 2000;49:1-9.
7. Werner CM and Bohm M. The therapeutic role of RAS blockade in chronic heart failure. *Ther Adv Cardiovasc Dis*. 2008;2:167-77.
8. Moen JM, Matt MG, Ramirez C, Tarasov KV, Chakir K, Tarasova YS, Lukyanenko Y, Tsutsui K, Monfredi O, Morrell CH, Tagirova S, Yaniv Y, Huynh T, Pacak K, Ahmet I and Lakatta EG. Overexpression of a Neuronal Type Adenylyl Cyclase (Type 8) in Sinoatrial Node Markedly Impacts Heart Rate and Rhythm. *Front Neurosci*. 2019;13:615.
9. Lipskaia L, Defer N, Esposito G, Hajar I, Garel MC, Rockman HA and Hanoune J. Enhanced Cardiac Function in Transgenic Mice Expressing a Ca2+-Stimulated Adenylyl Cyclase. *Circulation Research*. 2000;86:795-801.
10. Mougenot N, Mika D, Czibik G, Marcos E, Abid S, Houssaini A, Vallin B, Guellich A, Mehel H, Sawaki D, Vandecasteele G, Fischmeister R, Hajjar RJ, Dubois-Rande JL, Limon I, Adnot S, Derumeaux G and Lipskaia L. Cardiac adenylyl cyclase overexpression precipitates and aggravates age-related myocardial dysfunction. *Cardiovasc Res*. 2019;115:1778-1790.
11. Liu Y, Zhou K, Li J, Agvanian S, Caldaruse AM, Shaw S, Hitzeman TC, Shaw RM and Hong T. In Mice Subjected to Chronic Stress, Exogenous cBIN1 Preserves Calcium-Handling Machinery and Cardiac Function. *JACC Basic Transl Sci*. 2020;5:561-578.
12. Zhang GX, Kimura S, Nishiyama A, Shokoji T, Rahman M, Yao L, Nagai Y, Fujisawa Y, Miyatake A and Abe Y. Cardiac oxidative stress in acute and chronic isoproterenol-infused rats. *Cardiovasc Res*. 2005;65:230-8.
13. Georget M, Mateo P, Vandecasteele G, Jurevicius J, Lipskaia L, Defer N, Hanoune J, Hoerter J and Fischmeister R. Augmentation of cardiac contractility with no change in L-type Ca2+ current in transgenic mice with a cardiac-directed expression of the human adenylyl cyclase type 8 (AC8). *FASEB J*. 2002;16:1636-8.
14. Georget M, Mateo P, Vandecasteele G, Lipskaia L, Defer N, Hanoune J, Hoerter J, Lugnier C and Fischmeister R. Cyclic AMP compartmentation due to increased cAMP-phosphodiesterase activity in transgenic mice with a cardiac-directed expression of the human adenylyl cyclase type 8 (AC8). *FASEB J*. 2003;17:1380-91.

15. Hanahan D and Weinberg RA. The hallmarks of cancer. *Cell*. 2000;100:57-70.
16. Hanahan D and Weinberg RA. Hallmarks of cancer: the next generation. *Cell*. 2011;144:646-74.
17. Dorn GW, 2nd. The fuzzy logic of physiological cardiac hypertrophy. *Hypertension*. 2007;49:962-70.
18. Maillet M, van Berlo JH and Molkentin JD. Molecular basis of physiological heart growth: fundamental concepts and new players. *Nat Rev Mol Cell Biol*. 2013;14:38-48.
19. Wilkins BJ and Molkentin JD. Calcium-calcineurin signaling in the regulation of cardiac hypertrophy. *Biochem Biophys Res Commun*. 2004;322:1178-91.
20. Soonpaa MH, Koh GY, Klug MG and Field LJ. Formation of nascent intercalated disks between grafted fetal cardiomyocytes and host myocardium. *Science*. 1994;264:98-101.
21. Pinson A, Schluter KD, Zhou XJ, Schwartz P, Kessler-Icekson G and Piper HM. Alpha- and beta-adrenergic stimulation of protein synthesis in cultured adult ventricular cardiomyocytes. *J Mol Cell Cardiol*. 1993;25:477-90.
22. Yamazaki T, Komuro I, Zou Y, Kudoh S, Shiojima I, Hiroi Y, Mizuno T, Aikawa R, Takano H and Yazaki Y. Norepinephrine induces the raf-1 kinase/mitogen-activated protein kinase cascade through both alpha 1- and beta-adrenoceptors. *Circulation*. 1997;95:1260-8.
23. Zorov DB, Filburn CR, Klotz LO, Zweier JL and Sollott SJ. Reactive oxygen species (ROS)-induced ROS release: a new phenomenon accompanying induction of the mitochondrial permeability transition in cardiac myocytes. *J Exp Med*. 2000;192:1001-14.
24. Juhaszova M, Zorov DB, Kim SH, Pepe S, Fu Q, Fishbein KW, Ziman BD, Wang S, Ytrehus K, Antos CL, Olson EN and Sollott SJ. Glycogen synthase kinase-3beta mediates convergence of protection signaling to inhibit the mitochondrial permeability transition pore. *J Clin Invest*. 2004;113:1535-49.
25. Zorov DB, Juhaszova M and Sollott SJ. Mitochondrial reactive oxygen species (ROS) and ROS-induced ROS release. *Physiol Rev*. 2014;94:909-50.
26. Aon MA, Cortassa S, Juhaszova M, Gonzalez-Reyes JA, Calvo-Rubio M, Villalba JM, Lachance AD, Ziman BD, Mitchell SJ, Murt KN, Axsom JEC, Alfaras I, Britton SL, Koch LG, de Cabo R, Lakatta EG and Sollott SJ. Mitochondrial health is enhanced in rats with higher vs. lower intrinsic exercise capacity and extended lifespan. *NPJ Aging Mech Dis*. 2021;7:1.
27. Liebermeister W, Noor E, Flamholz A, Davidi D, Bernhardt J and Milo R. Visual account of protein investment in cellular functions. *Proc Natl Acad Sci U S A*. 2014;111:8488-93.
28. Vander Heiden MG, Cantley LC and Thompson CB. Understanding the Warburg effect: the metabolic requirements of cell proliferation. *Science*. 2009;324:1029-33.
29. Matsuura TR, Leone TC and Kelly DP. Fueling Cardiac Hypertrophy. *Circ Res*. 2020;126:197-199.
30. Ritterhoff J, Young S, Villet O, Shao D, Neto FC, Bettcher LF, Hsu YA, Kolwicz SC, Jr., Raftery D and Tian R. Metabolic Remodeling Promotes Cardiac Hypertrophy by Directing Glucose to Aspartate Biosynthesis. *Circ Res*. 2020;126:182-196.
31. Dorn GW, 2nd, Robbins J and Sugden PH. Phenotyping hypertrophy: eschew obfuscation. *Circ Res*. 2003;92:1171-5.
32. Gogiraju R, Schroeter MR, Bochenek ML, Hubert A, Munzel T, Hasenfuss G and Schafer K. Endothelial deletion of protein tyrosine phosphatase-1B protects against pressure overload-induced heart failure in mice. *Cardiovasc Res*. 2016;111:204-16.
33. Bostrom P, Mann N, Wu J, Quintero PA, Plovie ER, Panakova D, Gupta RK, Xiao C, MacRae CA, Rosenzweig A and Spiegelman BM. C/EBPbeta controls exercise-induced cardiac growth and protects against pathological cardiac remodeling. *Cell*. 2010;143:1072-83.
34. Fleg JL, Schulman S, O'Connor F, Becker LC, Gerstenblith G, Clulow JF, Renlund DG and Lakatta EG. Effects of acute beta-adrenergic receptor blockade on age-associated changes in cardiovascular performance during dynamic exercise. *Circulation*. 1994;90:2333-41.

35. Moore RL, Musch TI, Yelamarty RV, Scaduto RC, Jr., Semanchick AM, Elensky M and Cheung JY. Chronic exercise alters contractility and morphology of isolated rat cardiac myocytes. *Am J Physiol*. 1993;264:C1180-9.
36. Rose BA, Force T and Wang Y. Mitogen-activated protein kinase signaling in the heart: angels versus demons in a heart-breaking tale. *Physiol Rev*. 2010;90:1507-46.
37. Dixon RE, Hwang SJ, Kim BH, Sanders KM and Ward SM. Myosalpinx Contractions Are Essential for Egg Transport Along the Oviduct and Are Disrupted in Reproductive Tract Diseases. *Adv Exp Med Biol*. 2019;1124:265-294.
38. Stansfield WE, Andersen NM, Tang RH and Selzman CH. Periostin is a novel factor in cardiac remodeling after experimental and clinical unloading of the failing heart. *Ann Thorac Surg*. 2009;88:1916-21.
39. Zhao S, Wu H, Xia W, Chen X, Zhu S, Zhang S, Shao Y, Ma W, Yang D and Zhang J. Periostin expression is upregulated and associated with myocardial fibrosis in human failing hearts. *J Cardiol*. 2014;63:373-8.
40. Ikeda H, Shiojima I, Ozasa Y, Yoshida M, Holzenberger M, Kahn CR, Walsh K, Igarashi T, Abel ED and Komuro I. Interaction of myocardial insulin receptor and IGF receptor signaling in exercise-induced cardiac hypertrophy. *J Mol Cell Cardiol*. 2009;47:664-75.
41. Varga I, Polak S, Kyselovic J, Kachlik D, Danisovic L and Klein M. Recently Discovered Interstitial Cell Population of Telocytes: Distinguishing Facts from Fiction Regarding Their Role in the Pathogenesis of Diverse Diseases Called "Telocytopathies". *Medicina (Kaunas)*. 2019;55.
42. Esposito G, Perrino C, Ozaki T, Takaoka H, Defer N, Petretta MP, De Angelis MC, Mao L, Hanoune J, Rockman HA and Chiariello M. Increased myocardial contractility and enhanced exercise function in transgenic mice overexpressing either adenylyl cyclase 5 or 8. *Basic Res Cardiol*. 2008;103:22-30.
43. Fajardo VM, Feng I, Chen BY, Perez-Ramirez CA, Shi B, Clark P, Tian R, Lien CL, Pellegrini M, Christofk H, Nakano H and Nakano A. GLUT1 overexpression enhances glucose metabolism and promotes neonatal heart regeneration. *Sci Rep*. 2021;11:8669.
44. Smoak IW and Branch S. Glut-1 expression and its response to hypoglycemia in the embryonic mouse heart. *Anat Embryol (Berl)*. 2000;201:327-33.
45. Brosius FC, 3rd, Liu Y, Nguyen N, Sun D, Bartlett J and Schwaiger M. Persistent myocardial ischemia increases GLUT1 glucose transporter expression in both ischemic and non-ischemic heart regions. *J Mol Cell Cardiol*. 1997;29:1675-85.
46. Razeghi P, Young ME, Alcorn JL, Moravec CS, Frazier OH and Taegtmeyer H. Metabolic gene expression in fetal and failing human heart. *Circulation*. 2001;104:2923-31.
47. Wang KC, Botting KJ, Zhang S, McMillen IC, Brooks DA and Morrison JL. Akt signaling as a mediator of cardiac adaptation to low birth weight. *J Endocrinol*. 2017;233:R81-R94.
48. Sousa Fialho MDL, Abd Jamil AH, Stannard GA and Heather LC. Hypoxia-inducible factor 1 signalling, metabolism and its therapeutic potential in cardiovascular disease. *Biochim Biophys Acta Mol Basis Dis*. 2019;1865:831-843.
49. Krishnan J, Suter M, Windak R, Krebs T, Felley A, Montessuit C, Tokarska-Schlattner M, Aasum E, Bogdanova A, Perriard E, Perriard JC, Larsen T, Pedrazzini T and Krek W. Activation of a HIF1alpha-PPARgamma axis underlies the integration of glycolytic and lipid anabolic pathways in pathologic cardiac hypertrophy. *Cell Metab*. 2009;9:512-24.
50. West MD, Labat I, Sternberg H, Larocca D, Nasonkin I, Chapman KB, Singh R, Makarev E, Aliper A, Kazennov A, Alekseenko A, Shuvalov N, Cheskidova E, Alekseev A, Artemov A, Putin E, Mamoshina P, Pryanichnikov N, Larocca J, Copeland K, Izumchenko E, Korzinkin M and Zhavoronkov A. Use of deep neural network ensembles to identify embryonic-fetal transition markers: repression of COX7A1 in embryonic and cancer cells. *Oncotarget*. 2018;9:7796-7811.

51. Brooks GA. Mammalian fuel utilization during sustained exercise. *Comp Biochem Physiol B Biochem Mol Biol*. 1998;120:89-107.
52. Safer B, Smith CM and Williamson JR. Control of the transport of reducing equivalents across the mitochondrial membrane in perfused rat heart. *J Mol Cell Cardiol*. 1971;2:111-24.
53. Kane DA. Lactate oxidation at the mitochondria: a lactate-malate-aspartate shuttle at work. *Front Neurosci*. 2014;8:366.
54. O'Donnell JM, Kudej RK, LaNoue KF, Vatner SF and Lewandowski ED. Limited transfer of cytosolic NADH into mitochondria at high cardiac workload. *Am J Physiol Heart Circ Physiol*. 2004;286:H2237-42.
55. Robergs RA, Ghiasvand F and Parker D. Biochemistry of exercise-induced metabolic acidosis. *Am J Physiol Regul Integr Comp Physiol*. 2004;287:R502-16.
56. Yet SF, Tian R, Layne MD, Wang ZY, Maemura K, Solovyeva M, Ith B, Melo LG, Zhang L, Ingwall JS, Dzau VJ, Lee ME and Perrella MA. Cardiac-specific expression of heme oxygenase-1 protects against ischemia and reperfusion injury in transgenic mice. *Circ Res*. 2001;89:168-73.
57. Zhao Y, Zhang L, Qiao Y, Zhou X, Wu G, Wang L, Peng Y, Dong X, Huang H, Si L, Zhang X, Zhang L, Li J, Wang W, Zhou L and Gao X. Heme oxygenase-1 prevents cardiac dysfunction in streptozotocin-diabetic mice by reducing inflammation, oxidative stress, apoptosis and enhancing autophagy. *PLoS One*. 2013;8:e75927.
58. Cui M, Atmanli A, Morales MG, Tan W, Chen K, Xiao X, Xu L, Liu N, Bassel-Duby R and Olson EN. Nrf1 promotes heart regeneration and repair by regulating proteostasis and redox balance. *Nat Commun*. 2021;12:5270.
59. Vanhaesebroeck B, Guillermet-Guibert J, Graupera M and Bilanges B. The emerging mechanisms of isoform-specific PI3K signalling. *Nat Rev Mol Cell Biol*. 2010;11:329-41.
60. Nienaber JJ, Tachibana H, Naga Prasad SV, Esposito G, Wu D, Mao L and Rockman HA. Inhibition of receptor-localized PI3K preserves cardiac beta-adrenergic receptor function and ameliorates pressure overload heart failure. *J Clin Invest*. 2003;112:1067-79.
61. Naga Prasad SV, Laporte SA, Chamberlain D, Caron MG, Barak L and Rockman HA. Phosphoinositide 3-kinase regulates beta2-adrenergic receptor endocytosis by AP-2 recruitment to the receptor/beta-arrestin complex. *J Cell Biol*. 2002;158:563-75.
62. Patrucco E, Notte A, Barberis L, Selvetella G, Maffei A, Brancaccio M, Marengo S, Russo G, Azzolino O, Rybalkin SD, Silengo L, Altruda F, Wetzker R, Wymann MP, Lembo G and Hirsch E. PI3Kgamma modulates the cardiac response to chronic pressure overload by distinct kinase-dependent and -independent effects. *Cell*. 2004;118:375-87.
63. Perino A, Ghigo A, Damilano F and Hirsch E. Identification of the macromolecular complex responsible for PI3Kgamma-dependent regulation of cAMP levels. *Biochem Soc Trans*. 2006;34:502-3.
64. Morisco C, Zebrowski D, Condorelli G, Tsichlis P, Vatner SF and Sadoshima J. The Akt-glycogen synthase kinase 3beta pathway regulates transcription of atrial natriuretic factor induced by beta-adrenergic receptor stimulation in cardiac myocytes. *J Biol Chem*. 2000;275:14466-75.
65. Schluter KD, Goldberg Y, Taimor G, Schafer M and Piper HM. Role of phosphatidylinositol 3-kinase activation in the hypertrophic growth of adult ventricular cardiomyocytes. *Cardiovasc Res*. 1998;40:174-81.
66. Jo SH, Leblais V, Wang PH, Crow MT and Xiao RP. Phosphatidylinositol 3-kinase functionally compartmentalizes the concurrent G(s) signaling during beta2-adrenergic stimulation. *Circ Res*. 2002;91:46-53.
67. Leblais V, Jo SH, Chakir K, Maltsev V, Zheng M, Crow MT, Wang W, Lakatta EG and Xiao RP. Phosphatidylinositol 3-kinase offsets cAMP-mediated positive inotropic effect via inhibiting Ca2+ influx in cardiomyocytes. *Circ Res*. 2004;95:1183-90.

68. Oudit GY, Crackower MA, Eriksson U, Sarao R, Kozieradzki I, Sasaki T, Irie-Sasaki J, Gidrewicz D, Rybin VO, Wada T, Steinberg SF, Backx PH and Penninger JM. Phosphoinositide 3-kinase gamma-deficient mice are protected from isoproterenol-induced heart failure. *Circulation*. 2003;108:2147-52.
69. Lips DJ, Bueno OF, Wilkins BJ, Purcell NH, Kaiser RA, Lorenz JN, Voisin L, Saba-El-Leil MK, Meloche S, Pouyssegur J, Pages G, De Windt LJ, Doevendans PA and Molkentin JD. MEK1-ERK2 signaling pathway protects myocardium from ischemic injury in vivo. *Circulation*. 2004;109:1938-41.
70. Bassat E, Mutlak YE, Genzelinakh A, Shadrin IY, Baruch Umansky K, Yifa O, Kain D, Rajchman D, Leach J, Riabov Bassat D, Udi Y, Sarig R, Sagi I, Martin JF, Bursac N, Cohen S and Tzahor E. The extracellular matrix protein agrin promotes heart regeneration in mice. *Nature*. 2017;547:179-184.
71. de Jonge N, Goumans MJ, Lips D, Hassink R, Vlug EJ, van der Meel R, Emmerson CD, Nijman J, de Windt L and Doevendans PA. Controlling cardiomyocyte survival. *Novartis Found Symp*. 2006;274:41-51; discussion 51-7, 152-5, 272-6.
72. DeBosch B, Treskov I, Lupu TS, Weinheimer C, Kovacs A, Courtois M and Muslin AJ. Akt1 is required for physiological cardiac growth. *Circulation*. 2006;113:2097-104.
73. Antos CL, McKinsey TA, Frey N, Kutschke W, McAnally J, Shelton JM, Richardson JA, Hill JA and Olson EN. Activated glycogen synthase-3 beta suppresses cardiac hypertrophy in vivo. *Proc Natl Acad Sci U S A*. 2002;99:907-12.
74. Moc C, Taylor AE, Chesini GP, Zambrano CM, Barlow MS, Zhang X, Gustafsson AB and Purcell NH. Physiological activation of Akt by PHLPP1 deletion protects against pathological hypertrophy. *Cardiovasc Res*. 2015;105:160-70.
75. Freed DH, Borowiec AM, Angelovska T and Dixon IM. Induction of protein synthesis in cardiac fibroblasts by cardiotrophin-1: integration of multiple signaling pathways. *Cardiovasc Res*. 2003;60:365-75.
76. Das S, Dixon JE and Cho W. Membrane-binding and activation mechanism of PTEN. *Proc Natl Acad Sci U S A*. 2003;100:7491-6.
77. Torres J and Pulido R. The tumor suppressor PTEN is phosphorylated by the protein kinase CK2 at its C terminus. Implications for PTEN stability to proteasome-mediated degradation. *J Biol Chem*. 2001;276:993-8.
78. Vazquez F, Ramaswamy S, Nakamura N and Sellers WR. Phosphorylation of the PTEN tail regulates protein stability and function. *Mol Cell Biol*. 2000;20:5010-8.
79. Czech MP. PIP2 and PIP3: complex roles at the cell surface. *Cell*. 2000;100:603-6.
80. Yang B, Yan P, Gong H, Zuo L, Shi Y, Guo J, Guo R, Xie J and Li B. TWEAK protects cardiomyocyte against apoptosis in a PI3K/AKT pathway dependent manner. *Am J Transl Res*. 2016;8:3848-3860.
81. Abeyrathna P and Su Y. The critical role of Akt in cardiovascular function. *Vascul Pharmacol*. 2015;74:38-48.
82. Ghigo A and Li M. Phosphoinositide 3-kinase: friend and foe in cardiovascular disease. *Front Pharmacol*. 2015;6:169.
83. Khalil H, Bertrand MJ, Vandenabeele P and Widmann C. Caspase-3 and RasGAP: a stress-sensing survival/demise switch. *Trends Cell Biol*. 2014;24:83-9.
84. Choi J, Park JE, Tsagkogeorga G, Yanagita M, Koo BK, Han N and Lee JH. Inflammatory Signals Induce AT2 Cell-Derived Damage-Associated Transient Progenitors that Mediate Alveolar Regeneration. *Cell Stem Cell*. 2020;27:366-382 e7.
85. Lindborg JA, Tran NM, Chenette DM, DeLuca K, Foli Y, Kannan R, Sekine Y, Wang X, Wollan M, Kim IJ, Sanes JR and Strittmatter SM. Optic nerve regeneration screen identifies multiple genes restricting adult neural repair. *Cell Rep*. 2021;34:108777.
86. Pradervand S, Yasukawa H, Muller OG, Kjekshus H, Nakamura T, St Amand TR, Yajima T, Matsumura K, Duplain H, Iwatate M, Woodard S, Pedrazzini T, Ross J, Firsov D, Rossier BC, Hoshijima M

and Chien KR. Small proline-rich protein 1A is a gp130 pathway- and stress-inducible cardioprotective protein. *EMBO J*. 2004;23:4517-25.
87. Shah H, Hacker A, Langburt D, Dewar M, McFadden MJ, Zhang H, Kuzmanov U, Zhou YQ, Hussain B, Ehsan F, Hinz B, Gramolini AO and Heximer SP. Myocardial Infarction Induces Cardiac Fibroblast Transformation within Injured and Noninjured Regions of the Mouse Heart. *J Proteome Res*. 2021;20:2867-2881.
88. Steiner P, Kulangara K, Sarria JC, Glauser L, Regazzi R and Hirling H. Reticulon 1-C/neuroendocrine-specific protein-C interacts with SNARE proteins. *J Neurochem*. 2004;89:569-80.
89. van de Velde HJ, Roebroek AJ, Senden NH, Ramaekers FC and Van de Ven WJ. NSP-encoded reticulons, neuroendocrine proteins of a novel gene family associated with membranes of the endoplasmic reticulum. *J Cell Sci*. 1994;107 (Pt 9):2403-16.
90. Adamo L, Rocha-Resende C, Prabhu SD and Mann DL. Reappraising the role of inflammation in heart failure. *Nat Rev Cardiol*. 2020;17:269-285.
91. Adamo L, Staloch LJ, Rocha-Resende C, Matkovich SJ, Jiang W, Bajpai G, Weinheimer CJ, Kovacs A, Schilling JD, Barger PM, Bhattacharya D and Mann DL. Modulation of subsets of cardiac B lymphocytes improves cardiac function after acute injury. *JCI Insight*. 2018;3.
92. Juilland M and Thome M. Role of the CARMA1/BCL10/MALT1 complex in lymphoid malignancies. *Curr Opin Hematol*. 2016;23:402-9.
93. Craige SM, Chen K, Blanton RM, Keaney JF, Jr. and Kant S. JNK and cardiometabolic dysfunction. *Biosci Rep*. 2019;39.
94. Sadoshima J, Montagne O, Wang Q, Yang G, Warden J, Liu J, Takagi G, Karoor V, Hong C, Johnson GL, Vatner DE and Vatner SF. The MEKK1-JNK pathway plays a protective role in pressure overload but does not mediate cardiac hypertrophy. *J Clin Invest*. 2002;110:271-9.
95. Kaiser RA, Liang Q, Bueno O, Huang Y, Lackey T, Klevitsky R, Hewett TE and Molkentin JD. Genetic inhibition or activation of JNK1/2 protects the myocardium from ischemia-reperfusion-induced cell death in vivo. *J Biol Chem*. 2005;280:32602-8.
96. Wallace DC. Mitochondria and cancer. *Nat Rev Cancer*. 2012;12:685-98.
97. Juhaszova M, Rabuel C, Zorov DB, Lakatta EG and Sollott SJ. Protection in the aged heart: preventing the heart-break of old age? *Cardiovasc Res*. 2005;66:233-44.
98. Fulghum K and Hill BG. Metabolic Mechanisms of Exercise-Induced Cardiac Remodeling. *Front Cardiovasc Med*. 2018;5:127.
99. Cortassa S, Caceres V, Bell LN, O'Rourke B, Paolocci N and Aon MA. From metabolomics to fluxomics: a computational procedure to translate metabolite profiles into metabolic fluxes. *Biophys J*. 2015;108:163-72.

Figures

Figure 1

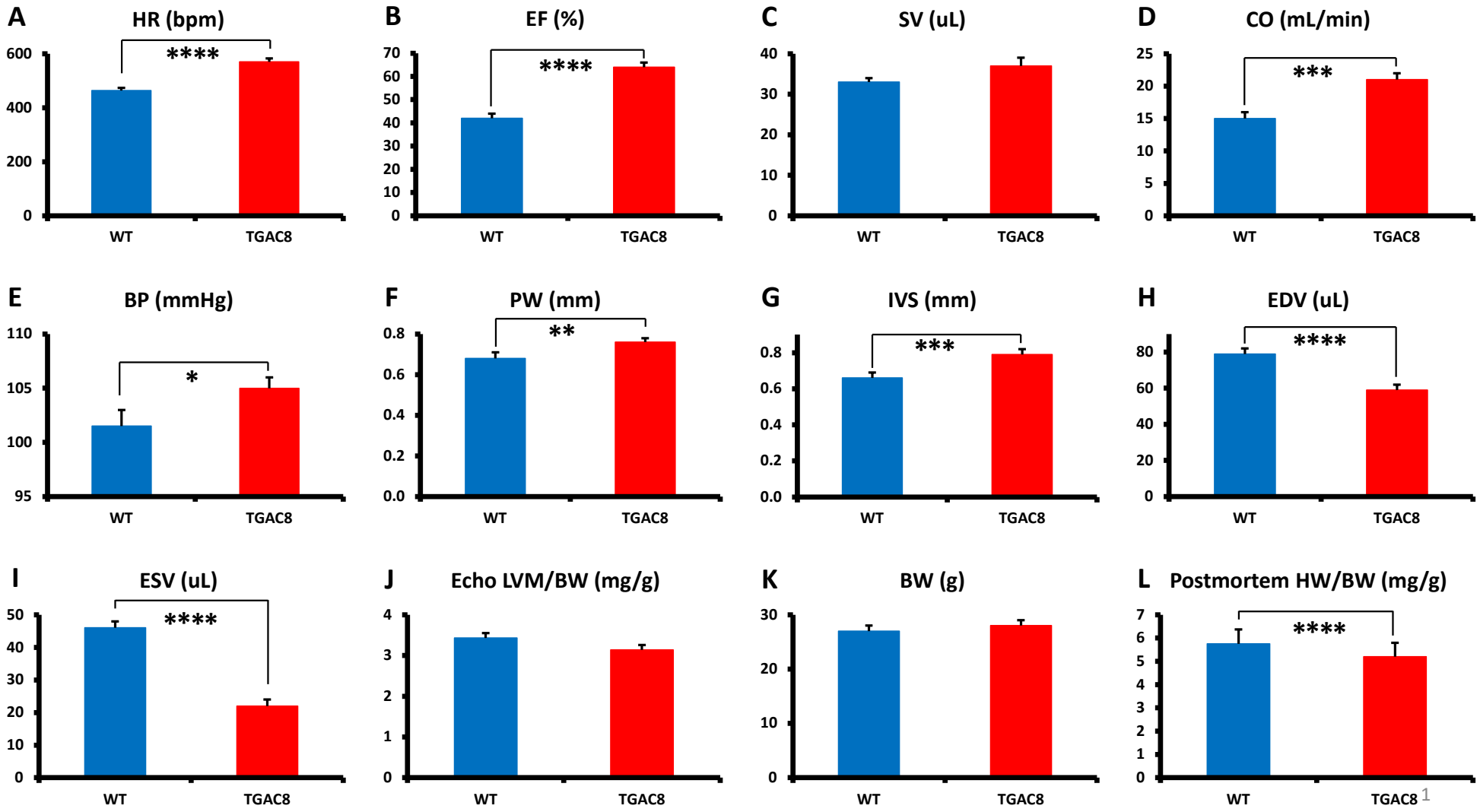
A
HR (bpm)
600
400
200
0
****
WT
TGAC8
B
EF (%)
70
60
50
40
30
20
10
0
****
WT
TGAC8
C
SV (uL)
40
30
20
10
0
WT
TGAC8
D
CO (mL/min)
25
20
15
10
5
0
***
WT
TGAC8
E
BP (mmHg)
110
105
100
95
*
WT
TGAC8
F
PW (mm)
0.8
0.6
0.4
0.2
0.0
**
WT
TGAC8
G
IVS (mm)
0.8
0.6
0.4
0.2
0.0
***
WT
TGAC8
H
EDV (uL)
80
60
40
20
0
****
WT
TGAC8
I
ESV (uL)
50
40
30
20
10
0
****
WT
TGAC8
J
Echo LVM/BW (mg/g)
4
3
2
1
0
WT
TGAC8
K
BW (g)
30
20
10
0
WT
TGAC8
L
Postmortem HW/BW (mg/g)
7
6
5
4
3
2
1
0
****
WT
TGAC8

Figure 2

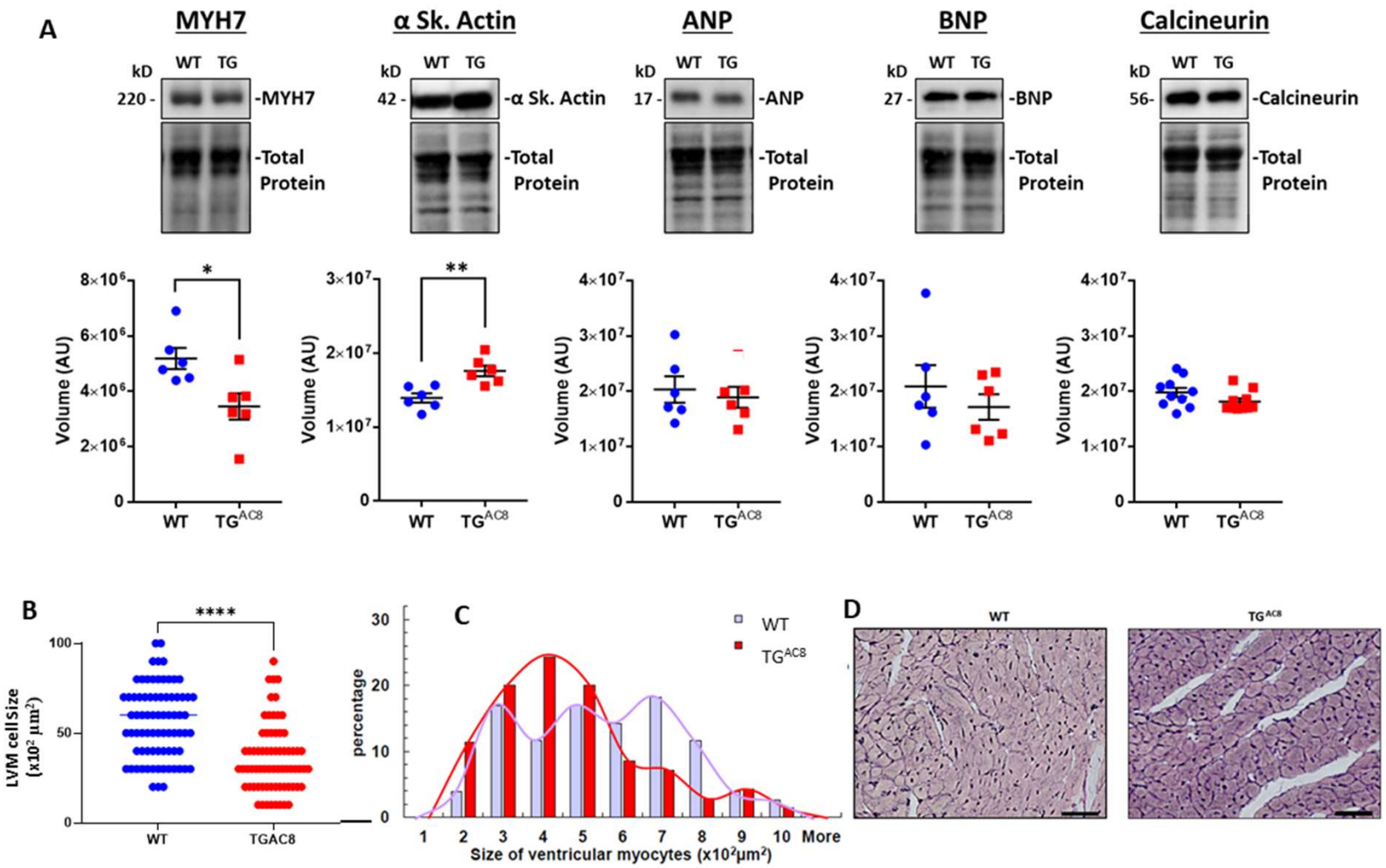
A
MYH7
α Sk. Actin
ANP
BNP
Calcineurin
kD
WT TG
220 -
-MYH7
42 -
-α Sk. Actin
17 -
-ANP
27 -
-BNP
56-
-Calcineurin
-Total Protein
Volume (AU)
WT
TGAC8
B
****
LVM cell Size (x10² µm²)
TGAC8
C
percentage
Size of ventricular myocytes (x10²µm²)
More
D

Figure 3

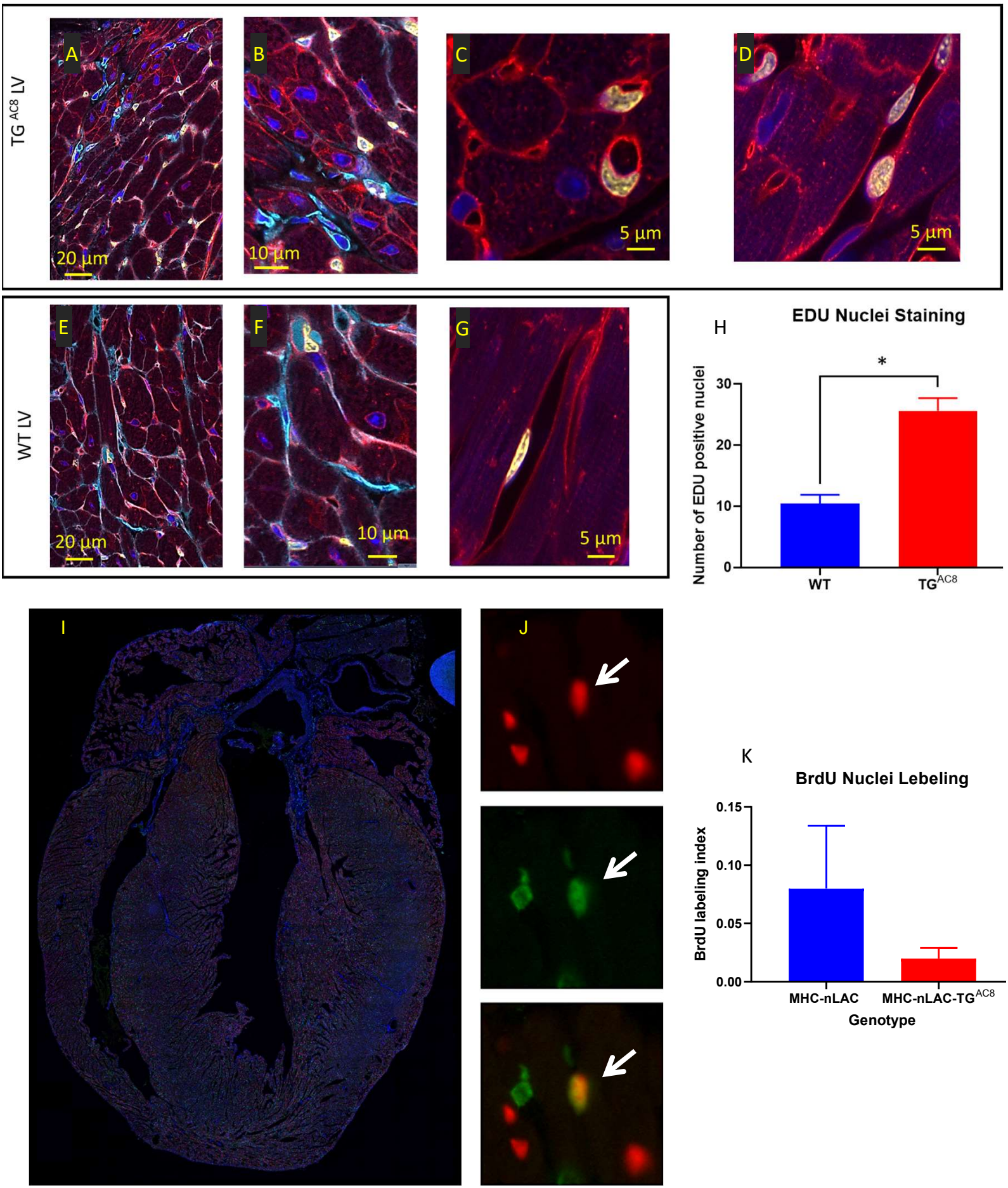
TG AC8 LV
A
20 µm
B
10 µm
C
5 µm
D
5 µm
WT LV
E
20 µm
F
10 µm
G
5 µm
H
EDU Nuclei Staining
Number of EDU positive nuclei
30
20
10
0
*
WT
TG AC8
I
J
K
BrdU Nuclei Lebeling
BrdU labeling index
0.15
0.10
0.05
0.00
MHC-nLAC
MHC-nLAC-TG AC8
Genotype

Figure 4

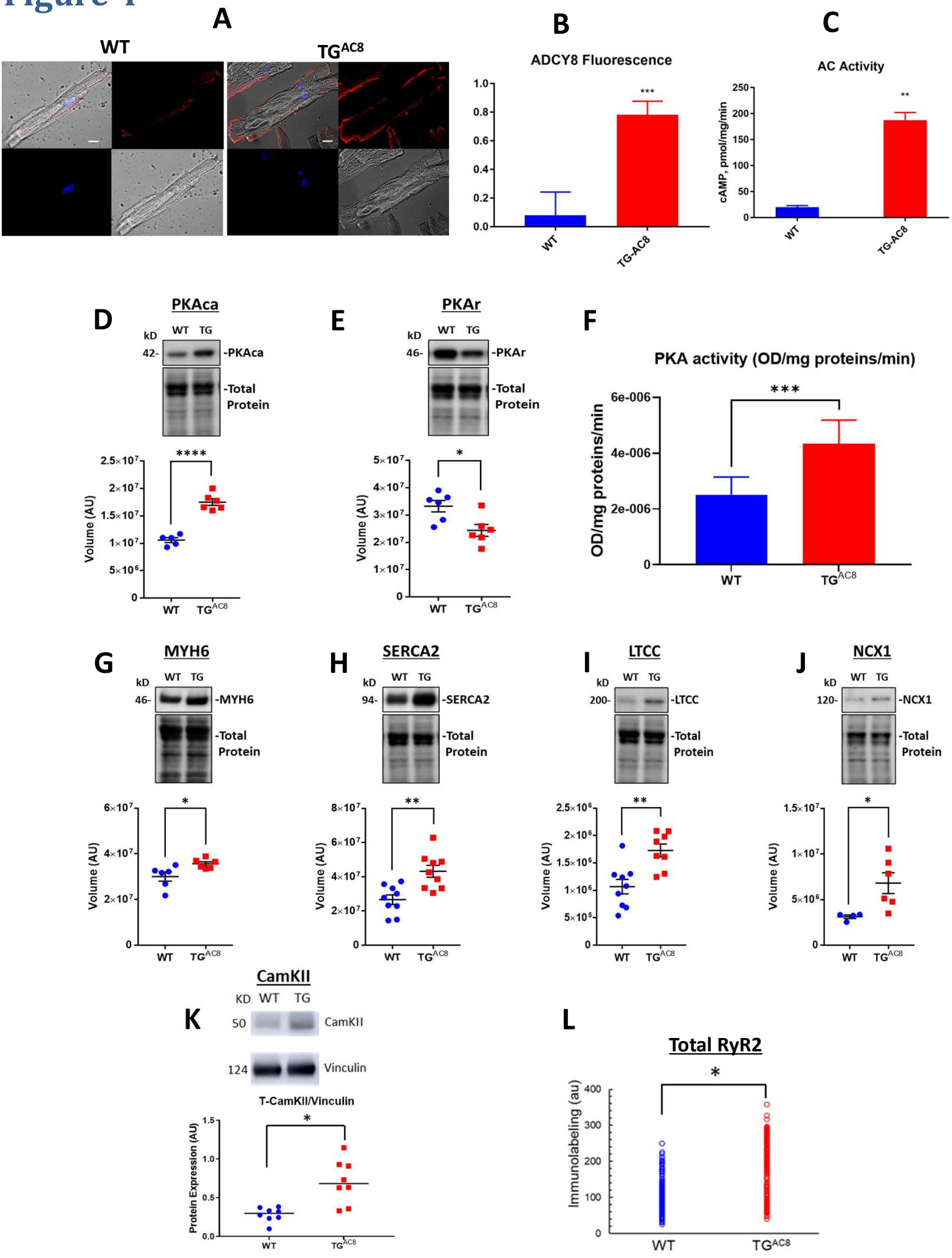
A
WT
TGAC8
B
ADCY8 Fluorescence
***
WT
TG-AC8
C
AC Activity
cAMP, pmol/mg/min
**
WT
TG-AC8
D
PKAca
kD
WT TG
42-
-PKAca
-Total Protein
****
Volume (AU)
WT
TGAC8
E
PKAr
kD
WT TG
46-
-PKAr
-Total Protein
*
Volume (AU)
WT
TGAC8
F
PKA activity (OD/mg proteins/min)
***
OD/mg proteins/min
WT
TGAC8
G
MYH6
kD
WT TG
46-
-MYH6
-Total Protein
*
Volume (AU)
WT
TGAC8
H
SERCA2
kD
WT TG
94-
-SERCA2
-Total Protein
**
Volume (AU)
WT
TGAC8
I
LTCC
kD
WT TG
200-
-LTCC
-Total Protein
**
Volume (AU)
WT
TGAC8
J
NCX1
kD
WT TG
120-
-NCX1
-Total Protein
*
Volume (AU)
WT
TGAC8
K
CamKII
KD
WT TG
50
CamKII
124
Vinculin
T-CamKII/Vinculin
*
Protein Expression (AU)
WT
TGAC8
L
Total RyR2
*
Immunolabeling (au)
WT
TGAC8

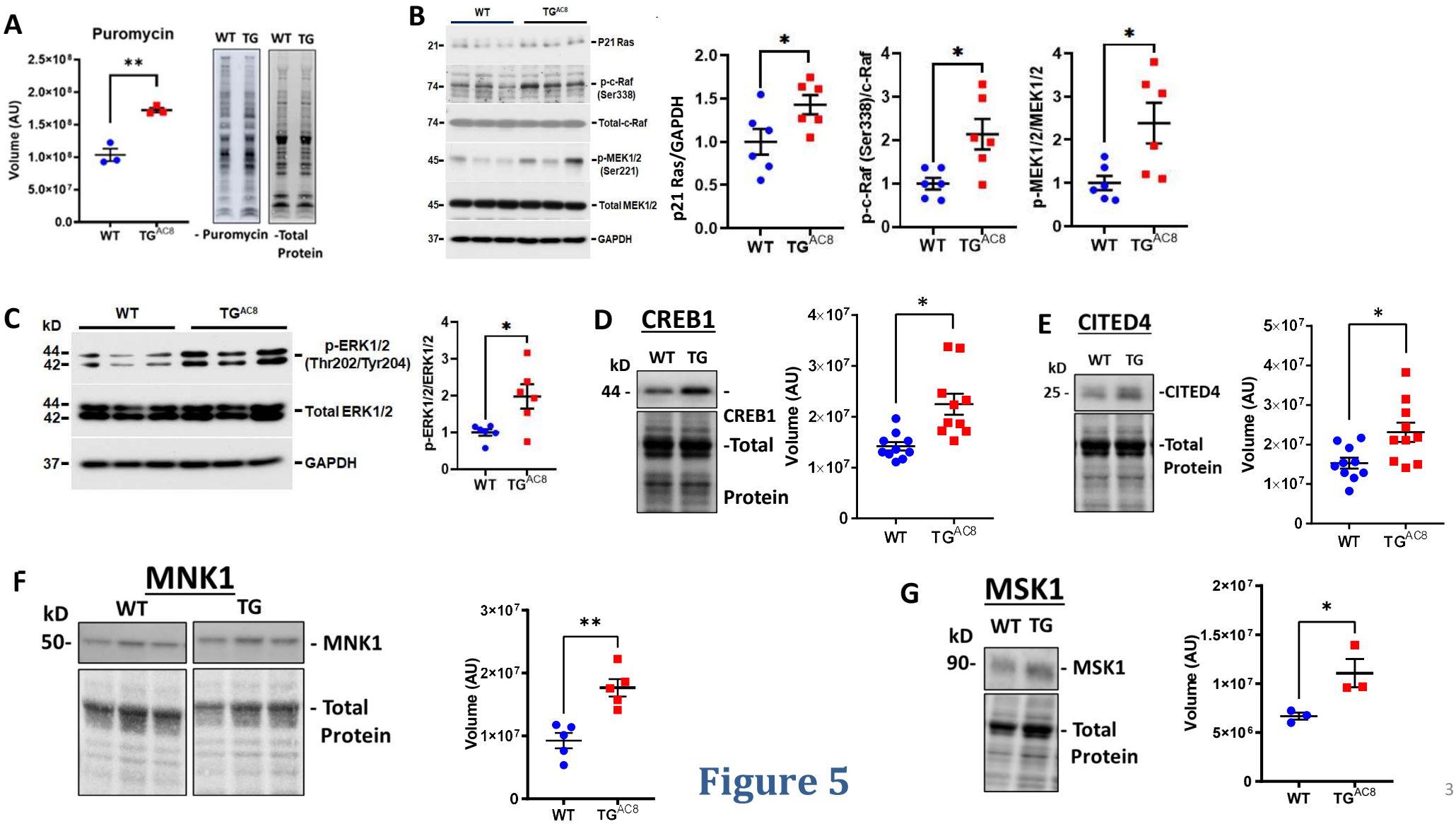
A
Puromycin
Volume (AU)
WT
TGAC8
- Puromycin
-Total Protein
B
P21 Ras
p-c-Raf (Ser338)
Total-c-Raf
p-MEK1/2 (Ser221)
Total MEK1/2
GAPDH
p21 Ras/GAPDH
p-c-Raf (Ser338)/c-Raf
p-MEK1/2/MEK1/2
C
kD
p-ERK1/2 (Thr202/Tyr204)
Total ERK1/2
GAPDH
p-ERK1/2/ERK1/2
D
CREB1
-Total Protein
E
CITED4
-CITED4
-Total Protein
F
MNK1
- MNK1
- Total Protein
G
MSK1
- MSK1
- Total Protein

Figure 5

Figure 6

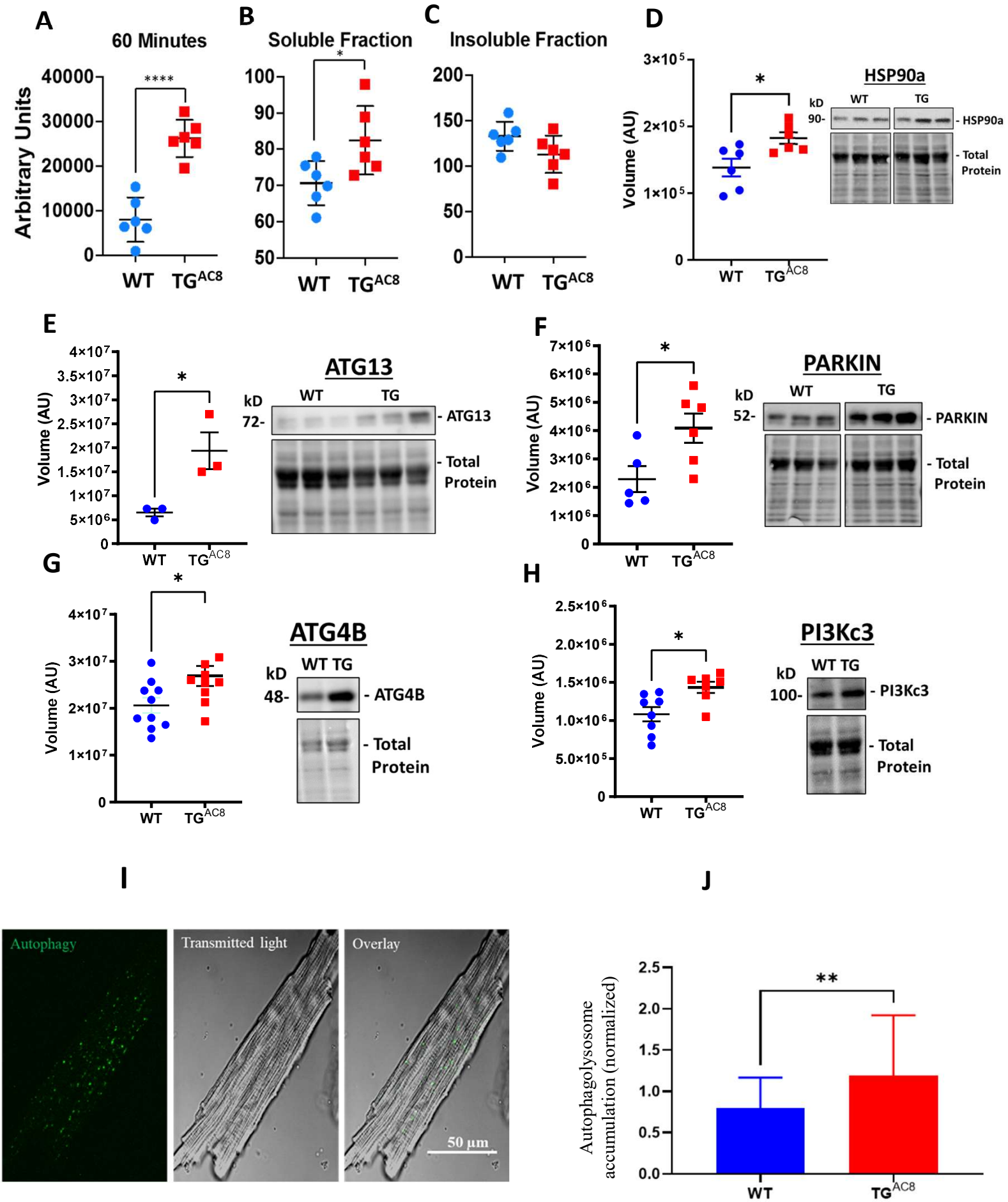
A
60 Minutes
Arbitrary Units
40000
30000
20000
10000
0
****
WT
TGAC8
B
Soluble Fraction
100
90
80
70
60
50
*
WT
TGAC8
C
Insoluble Fraction
200
150
100
50
0
WT
TGAC8
D
3×10^5
2×10^5
1×10^5
0
Volume (AU)
*
WT
TGAC8
HSP90a
kD
90-
WT
TG
- HSP90a
- Total Protein
E
4×10^7
3.5×10^7
3×10^7
2.5×10^7
2×10^7
1.5×10^7
1×10^7
5×10^6
0
Volume (AU)
*
WT
TGAC8
ATG13
kD
72-
WT
TG
- ATG13
- Total Protein
F
7×10^6
6×10^6
5×10^6
4×10^6
3×10^6
2×10^6
1×10^6
0
Volume (AU)
*
WT
TGAC8
PARKIN
kD
52-
WT
TG
- PARKIN
- Total Protein
G
4×10^7
3×10^7
2×10^7
1×10^7
0
Volume (AU)
*
WT
TGAC8
ATG4B
kD
48-
WT TG
- ATG4B
- Total Protein
H
2.5×10^6
2.0×10^6
1.5×10^6
1.0×10^6
5.0×10^5
0
Volume (AU)
*
WT
TGAC8
PI3Kc3
kD
100-
WT TG
- PI3Kc3
- Total Protein
I
Autophagy
Transmitted light
Overlay
50 µm
J
Autophagolysosome accumulation (normalized)
2.5
2.0
1.5
1.0
0.5
0.0
**
WT
TGAC8

Figure 7

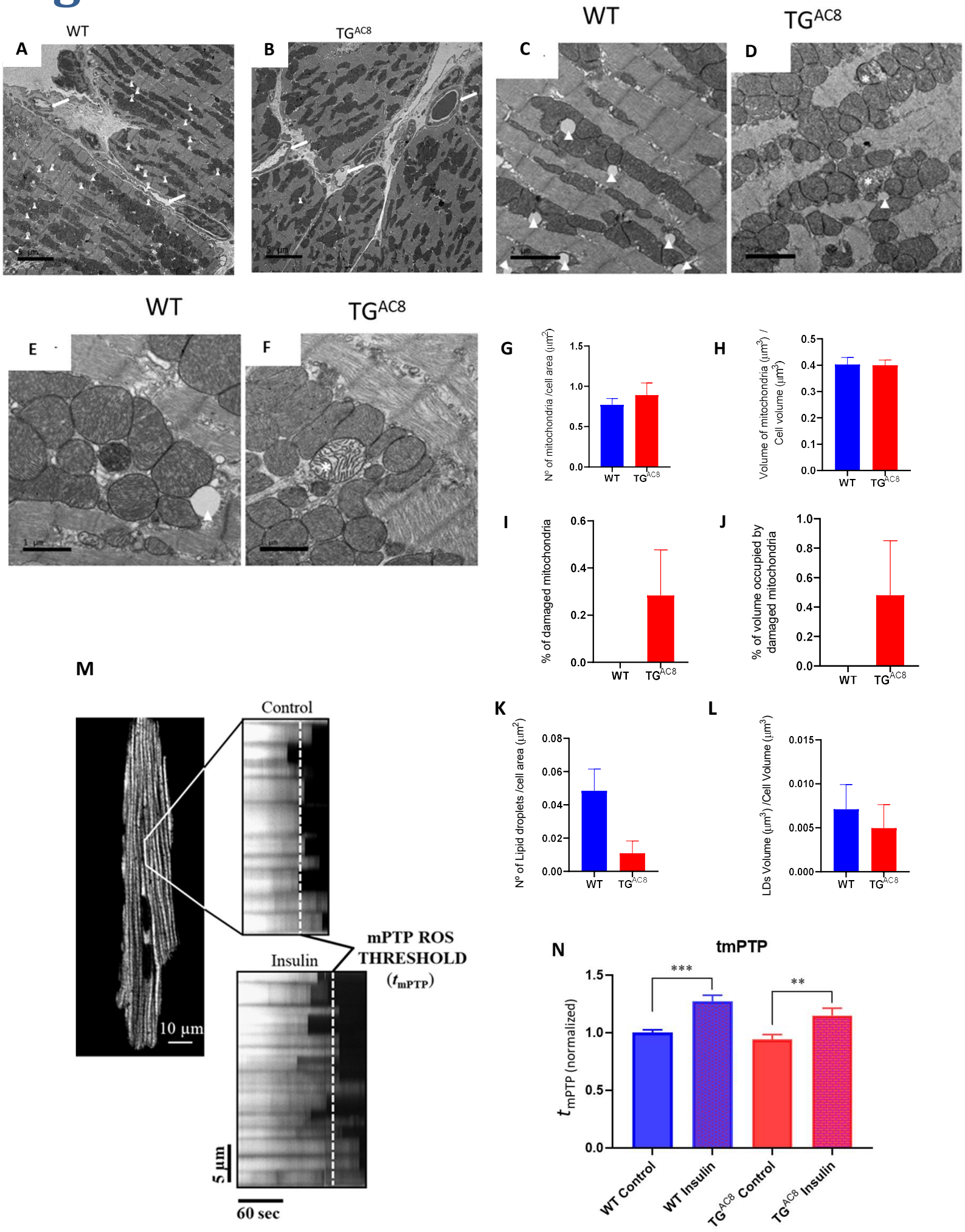
A
WT
B
TGAC8
C
WT
D
TGAC8
E
WT
F
TGAC8
G
Nº of mitochondria /cell area (µm2)
H
Volume of mitochondria (µm3) / Cell volume (µm3)
I
% of damaged mitochondria
J
% of volume occupied by damaged mitochondria
K
Nº of Lipid droplets /cell area (µm2)
L
LDs Volume (µm3) /Cell Volume (µm3)
M
Control
Insulin
mPTP ROS THRESHOLD (t_{mPTP})
10 µm
5 µm
60 sec
N
tmPTP
t_{mPTP} (normalized)
***
**
WT Control
WT Insulin
TGAC8 Control
TGAC8 Insulin

Figure 8

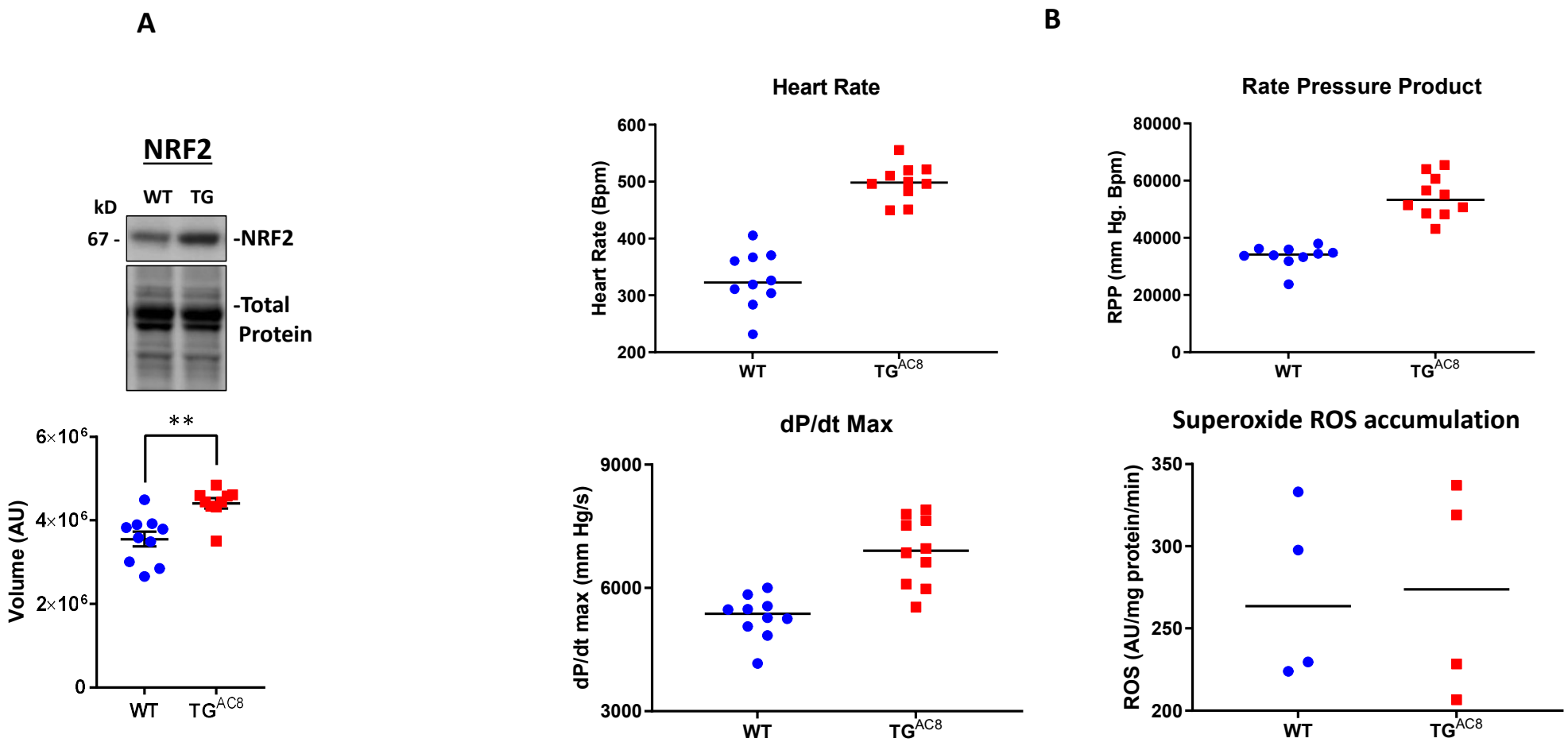
A
NRF2
kD
WT
TG
67 -
-NRF2
-Total
Protein
**
6×10⁶
4×10⁶
2×10⁶
0
Volume (AU)
WT
TGAC8
B
Heart Rate
Heart Rate (Bpm)
600
500
400
300
200
WT
TGAC8
Rate Pressure Product
RPP (mm Hg. Bpm)
80000
60000
40000
20000
0
WT
TGAC8
dP/dt Max
dP/dt max (mm Hg/s)
9000
6000
3000
WT
TGAC8
Superoxide ROS accumulation
ROS (AU/mg protein/min)
350
300
250
200
WT
TGAC8

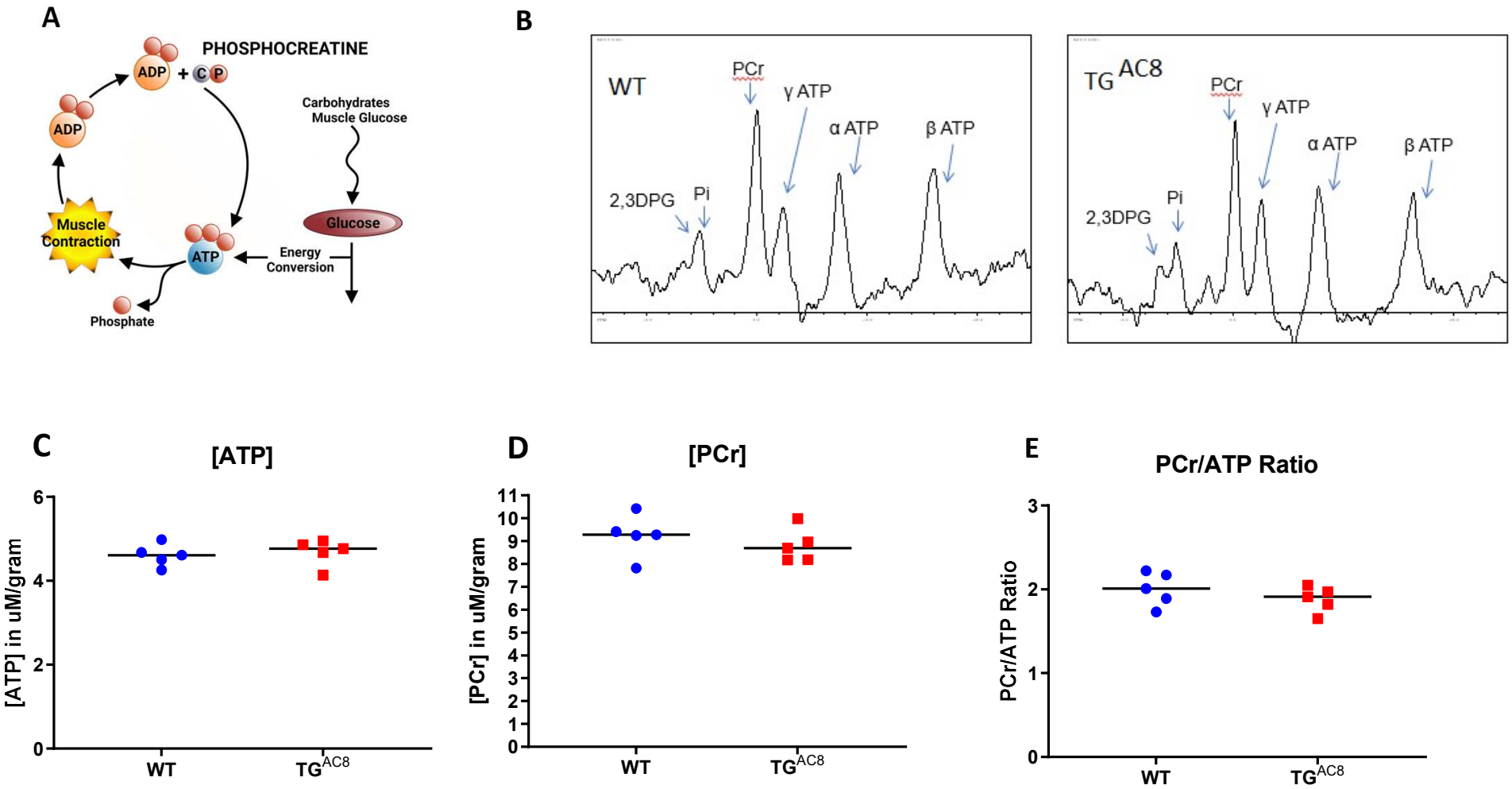
A
PHOSPHOCREATINE
ADP
+ C P
ADP
Carbohydrates
Muscle Glucose
Muscle Contraction
ATP
Glucose
Energy Conversion
Phosphate
B
WT
PCr
γ ATP
α ATP
β ATP
2,3DPG
Pi
TG AC8
PCr
γ ATP
α ATP
β ATP
2,3DPG
Pi
C
[ATP]
[ATP] in uM/gram
0
2
4
6
WT
TGAC8
D
[PCr]
[PCr] in uM/gram
0
1
2
3
4
5
6
7
8
9
10
11
WT
TGAC8
E
PCr/ATP Ratio
PCr/ATP Ratio
0
1
2
3
WT
TGAC8

Figure 9

Figure 10

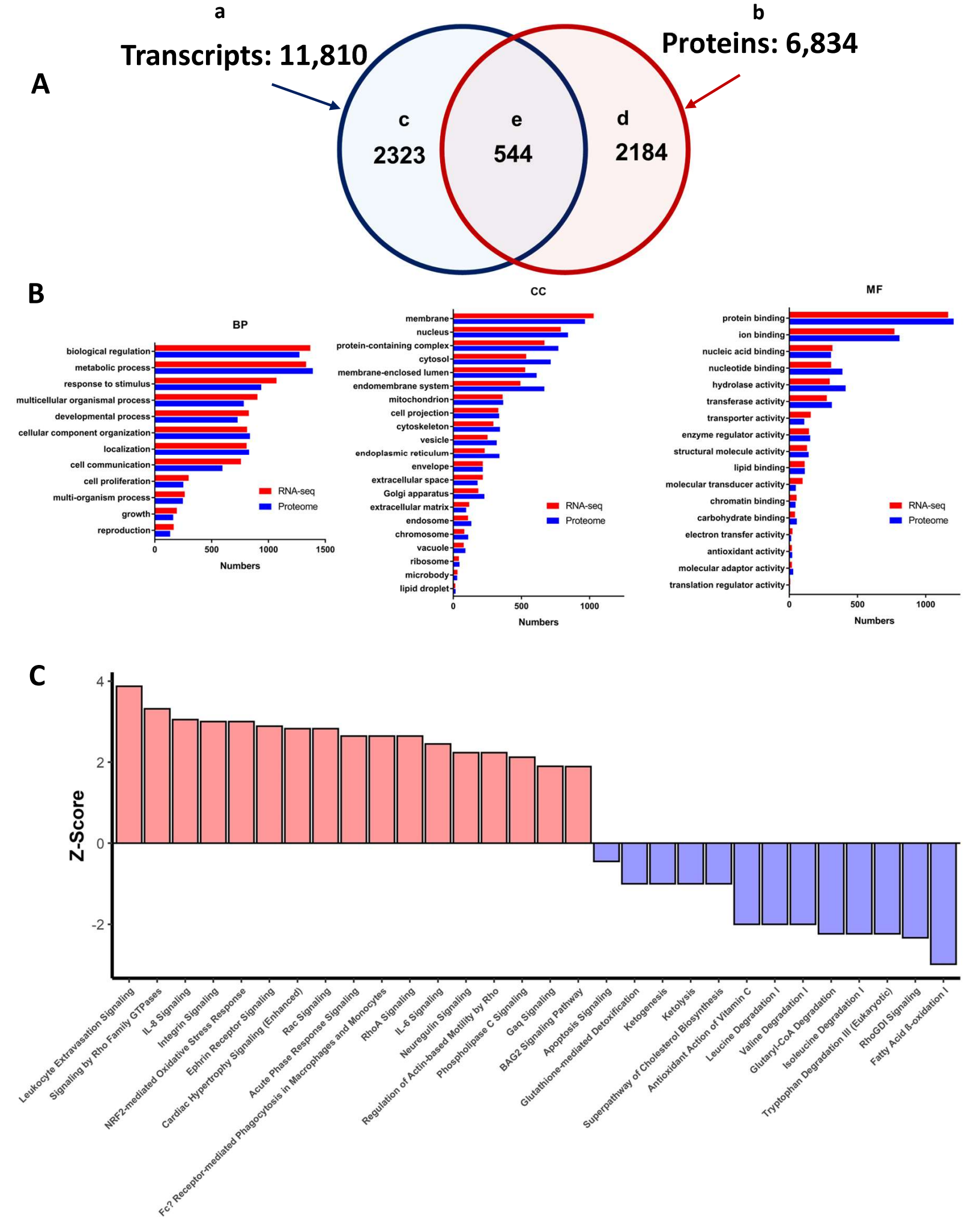
A
a
Transcripts: 11,810
b
Proteins: 6,834
c
2323
e
544
d
2184
B
BP
biological regulation
metabolic process
response to stimulus
multicellular organismal process
developmental process
cellular component organization
localization
cell communication
cell proliferation
multi-organism process
growth
reproduction
RNA-seq
Proteome
0
500
1000
1500
Numbers
CC
membrane
nucleus
protein-containing complex
cytosol
membrane-enclosed lumen
endomembrane system
mitochondrion
cell projection
cytoskeleton
vesicle
endoplasmic reticulum
envelope
extracellular space
Golgi apparatus
extracellular matrix
endosome
chromosome
vacuole
ribosome
microbody
lipid droplet
RNA-seq
Proteome
0
500
1000
Numbers
MF
protein binding
ion binding
nucleic acid binding
nucleotide binding
hydrolase activity
transferase activity
transporter activity
enzyme regulator activity
structural molecule activity
lipid binding
molecular transducer activity
chromatin binding
carbohydrate binding
electron transfer activity
antioxidant activity
molecular adaptor activity
translation regulator activity
RNA-seq
Proteome
0
500
1000
Numbers
C
Z-Score
4
2
0
-2
Leukocyte Extravasation Signaling
Signaling by Rho Family GTPases
IL-8 Signaling
Integrin Signaling
NRF2-mediated Oxidative Stress Response
Ephrin Receptor Signaling
Cardiac Hypertrophy Signaling (Enhanced)
Rac Signaling
Acute Phase Response Signaling
Fc? Receptor-mediated Phagocytosis in Macrophages and Monocytes
RhoA Signaling
IL-6 Signaling
Neuregulin Signaling
Regulation of Actin-based Motility by Rho
Phospholipase C Signaling
Gaq Signaling
BAG2 Signaling Pathway
Apoptosis Signaling
Glutathione-mediated Detoxification
Ketogenesis
Ketolysis
Superpathway of Cholesterol Biosynthesis
Antioxidant Action of Vitamin C
Leucine Degradation I
Valine Degradation I
Glutaryl-CoA Degradation
Isoleucine Degradation I
Tryptophan Degradation III (Eukaryotic)
RhoGDI Signaling
Fatty Acid ß-oxidation I

Figure 11

Regulatory Networks Centered on Adenylyl Cyclase and Protein Kinase A Signaling.

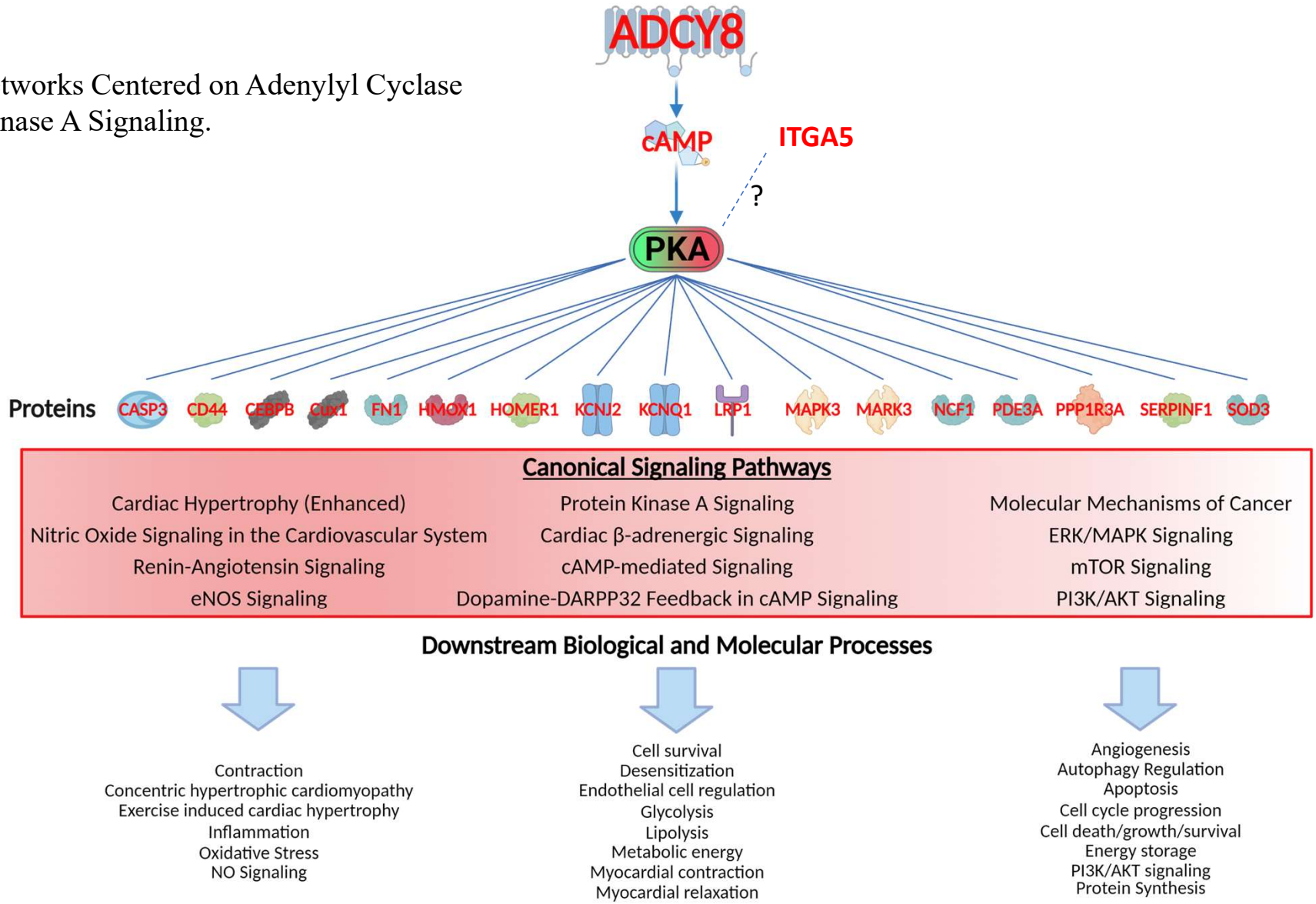

Figure 12

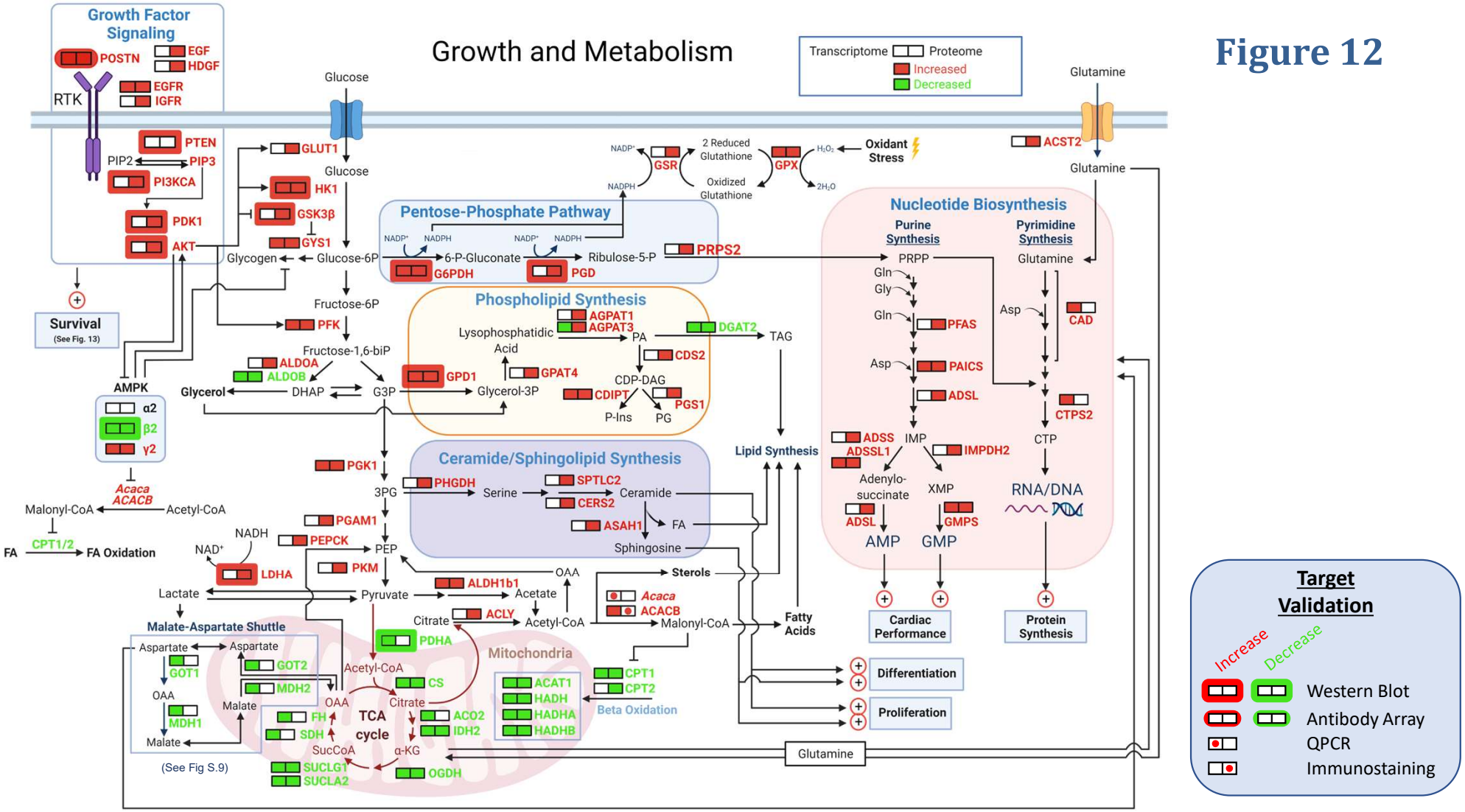

Created with BioRender.com

Figure 13
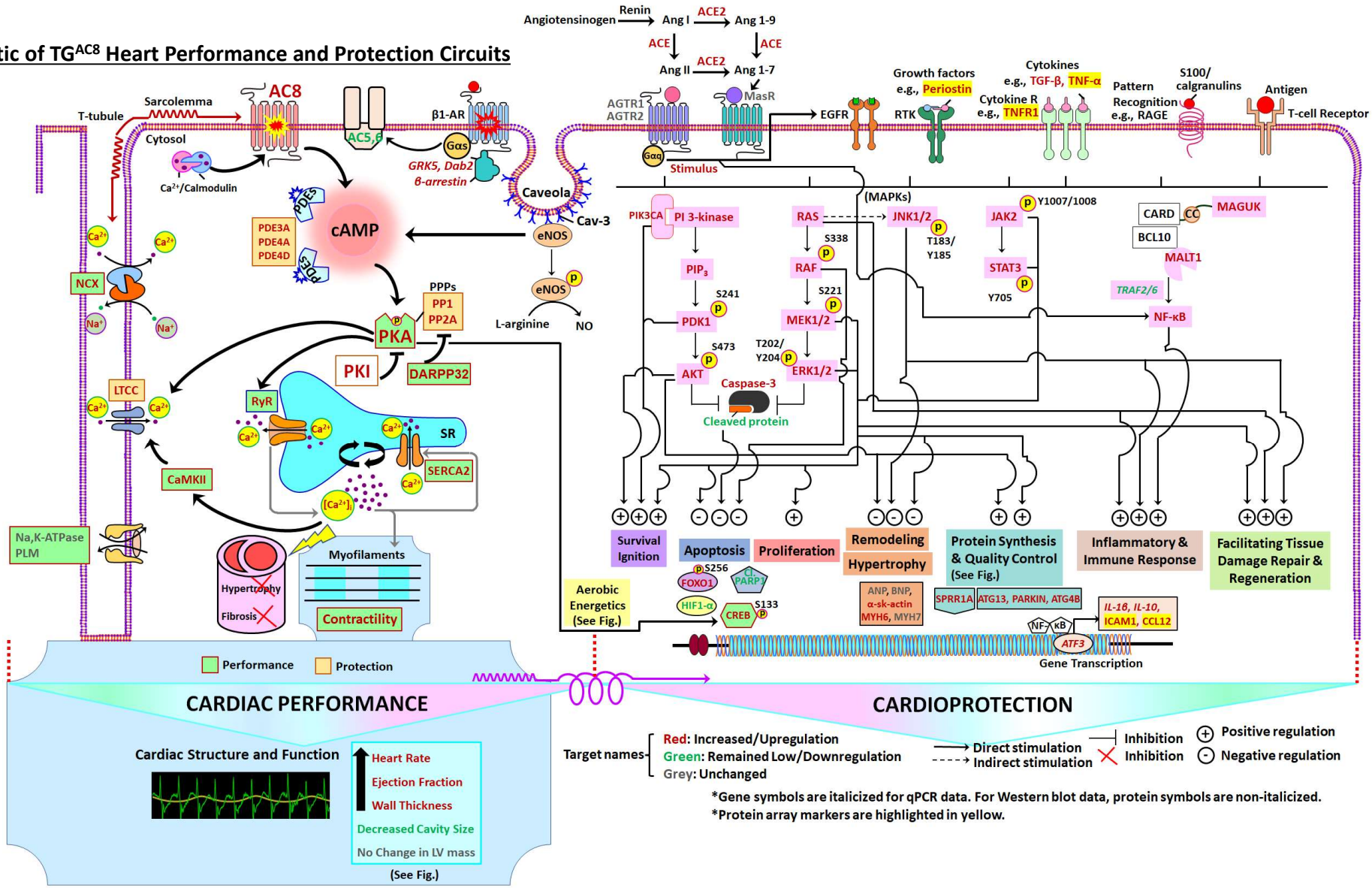
A Schematic of TG^{AC8} Heart Performance and Protection Circuits